

# We are IntechOpen, the world's leading publisher of Open Access books Built by scientists, for scientists

6,300

Open access books available

171,000

International authors and editors

190M

Downloads

Our authors are among the

154

Countries delivered to

TOP 1%

most cited scientists

12.2%

Contributors from top 500 universities



WEB OF SCIENCE™

Selection of our books indexed in the Book Citation Index  
in Web of Science™ Core Collection (BKCI)

Interested in publishing with us?  
Contact [book.department@intechopen.com](mailto:book.department@intechopen.com)

Numbers displayed above are based on latest data collected.  
For more information visit [www.intechopen.com](http://www.intechopen.com)



# Treatment of Water and Wastewater for Reuse and Energy Generation-Emerging Technologies

*Emmanuel Kweinor Tetteh, Sudesh Rathilal, Maggie Chetty, Edward Kwaku Armah and Dennis Asante-Sackey*

## Abstract

Fresh water quality and supply, particularly for domestic and industrial purposes, are deteriorating with contamination threats on water resources. Multiple technologies in the conventional wastewater treatment (WWT) settings have been adopted to purify water to a desirable quality. However, the design and selection of a suitable cost-effective treatment scheme for a catchment area are essential and have many considerations including land availability, energy, effluent quality and operational simplicity. Three emerging technologies are discussed, including anaerobic digestion, advanced oxidation processes (AOPs) and membrane technology, which holds great promise to provide integrational alternatives for manifold WWT process and distribution systems to mitigate contaminants and meet acceptable limitations. The main applications, basic principles, merits and demerits of the aforementioned technologies are addressed in relation to their current limitations and future research needs in terms of renewable energy. Hence, the advancement in manufacturing industry along with WWT blueprints will enhance the application of these technologies for the sustainable management and conservation of water.

**Keywords:** anaerobic digestion, advanced oxidation processes, membrane technology, renewable energy

## 1. Introduction

Wastewater, which is the biggest waste stream from municipalities, petrochemical, pharmaceuticals, food, textile, agricultural, polymer and paper industries and so on contain high contaminants of oil and salts of organic and inorganic compounds [1–5]. This strikes as a major ecological problem with high environmental impacts when discharged into the ecosystem without proper treatment. Furthermore, the industrial revolution associated with demographic growth have increased the demand for freshwater supply, which is depleting the natural fresh water supply sources [3, 5], although wastewater can be treated through various physical, chemical and biological strategies [1–3]. Unfortunately, the current conventional wastewater treatment methods cannot eliminate the contaminants. In addition conventional wastewater treatment can be expensive. Therefore, the quest for clean water and

clean environment has resulted in various environmental protection agencies setting stringent discharge limits [3, 4]. Conversely, there are always variations in wastewater qualities which have different impacts on the environment [2–4], where a proper wastewater treatment incorporated with primary, secondary and advanced treatment strategies seems to more viable [1, 3, 4]. The primary treatment involves separating the solids from the liquids via filtration or sedimentation, whereas the secondary treatment removes the dissolved solids and other contaminants through chemical precipitation and biological process [4, 6, 7]. Then UV light or membranes are used for further treatment [1, 2, 5]. After which, the treated water can be profitable to farmers as well as the environment positively in sustainable manner viz. irrigation, and agricultural purposes. In this study, evaluating the streamline flow of innovative wastewater treatment technologies for reuse and subsequent sludge generation as an energy source is being addressed. The biological treatment is presented in section one, followed by membrane technology and lastly the advanced oxidation process. The current limitations and future prospects of each technology are also presented.

## 2. The biological wastewater treatment process

Municipal solid wastes are attracting more obstructive legislation with respect to landfill disposal of the biodegradable fraction [4, 8]. The treatment process for these organic fractions is biological wastewater treatment. These technologies maximises the recycling and recovery processes of waste components. The biological treatment is regarded as an important and vital aspect of wastewater treatment and is a technique employed for municipal or industrial use for soluble organic components [9]. Among all, the most widely employed method for sludge treatment is anaerobic digestion [9, 10].

### 2.1 Anaerobic digestion (AD) process

In this process, a large fraction of the organic matter (cells) is broken down into carbon dioxide ( $\text{CO}_2$ ) and methane ( $\text{CH}_4$ ), and this is accomplished in the absence of oxygen. About half of the amount is then converted into gases, while the remainder is dried and becomes a residual soil-like material. Kougias and Angelidaki [11] reported that the end products of organic assimilation in anaerobic treatment of waste are  $\text{CH}_4$  and  $\text{CO}_2$  as depicted in **Figure 1**. The AD technology has encountered significant recognition in the last few decades with the applications of separately configured high rate treatment processes for industrial wastewater streams. In the wastewater treatment settings, the AD has been employed in several instances throughout the world for bioremediation and biogas production [8, 12, 13]. Biogas, a well-known and common renewable source of energy, is produced via the AD process, consisting largely of  $\text{CH}_4$  and  $\text{CO}_2$ . As an alternative source of energy, the AD process produces biogas that can be chiefly used as fuel in combined heat and power gas engines [11, 12, 14]. There has also been a rapid adoption of anaerobic co-digestion, where two or more different feed stocks are digested together in anaerobic biodigesters with the core aim of improving the biogas yield [8, 11–13, 15–17]. Other advantages ensured in the anaerobic systems include lower energy requirements, a safer and more convenient way of converting “waste” to useful products associated with urbanisation, being a predictive tool for the fulfilment of the UN Sustainability Goal to meet Global standards, having excellent nutrient recovery and high organic removal efficiencies. Drawbacks include longer hydraulic retention times (2–4 months) and high alkalinity requirements [11, 18, 19]. The aerobic system presents merits such as high organic removal efficiencies, excellent effluent quality

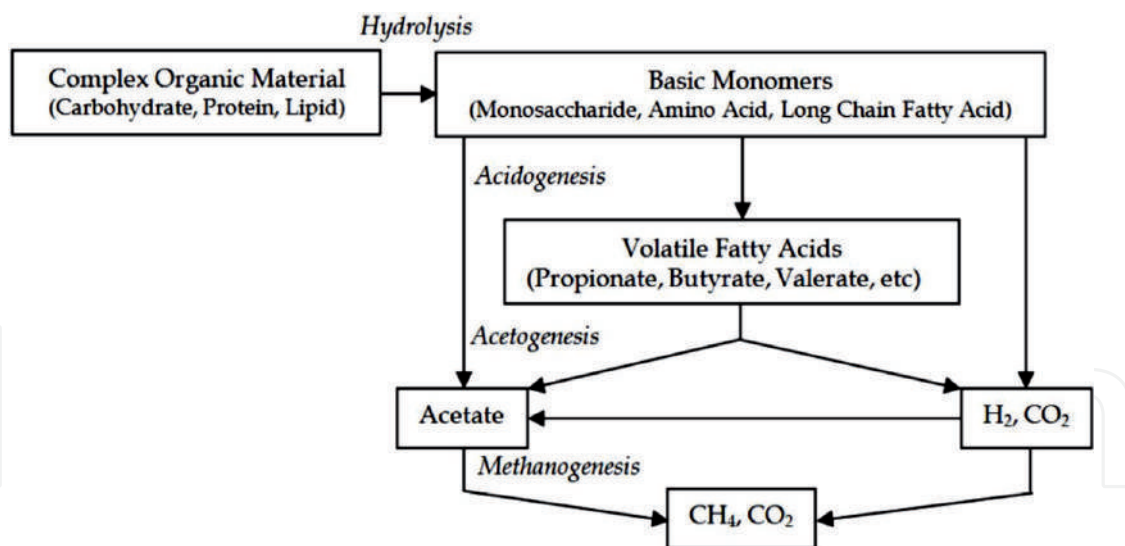


**Figure 1.**  
 Modified stages of the anaerobic digestion process, adapted from [11, 12].

and shorter start-up times (2–4 weeks). Demerits include longer hydraulic retention times, pretreatment requirements for delignification of lignocellulosic biomass, odour built-up in bioreactors, costs associated with CO<sub>2</sub> upgrading, no nutrient recovery and high energy requirements [8, 12, 17]. Research conducted by Kainthola et al. [19] details the major differences between the anaerobic and aerobic systems of wastewater treatments, as depicted in **Figure 2**, demonstrating the mechanism with species required and products formed. The anaerobic/aerobic systems have also been employed largely at both municipal and industrial levels as a method for wastewater treatment for many years. It presents advantages such as a lower consumption of energy, low chemical consumption, low sludge production, its enormous potential for the recovery of resources, simplicity of the operation and the requirement of less equipment. Some advantages of the biological treatment method over other treatment techniques such as thermal and chemical oxidations are capital investments required and costs in operation of the processes [8, 11, 12, 14].

### 2.1.1 Operating parameters of AD process

Some operating parameters which are usually monitored and optimised to maximise the performance and operation of AD include organic loading rate, pH, hydraulic

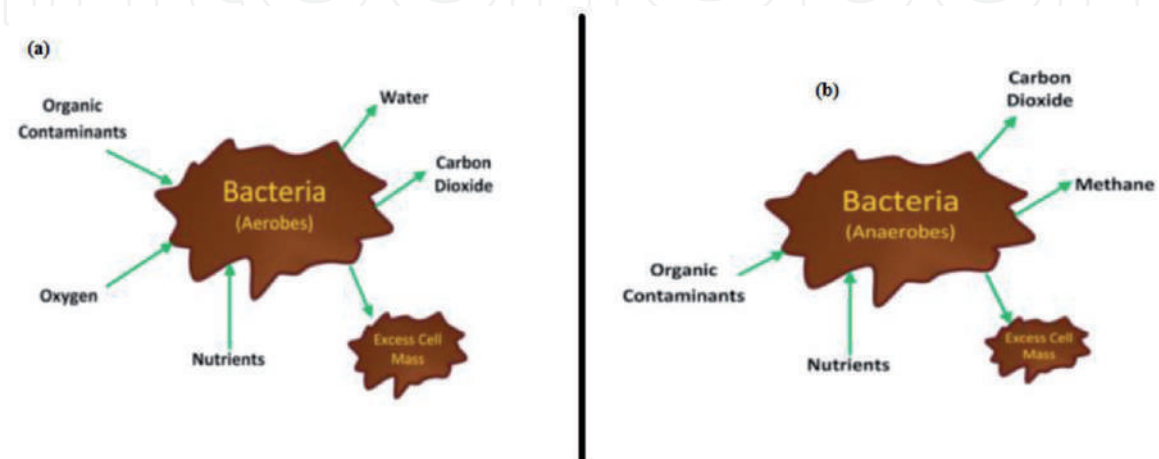


**Figure 2.**  
 Schematic diagrams of (a) aerobic treatment principle and (b) anaerobic treatment principle, adapted from [11, 12].

retention time, temperature, carbon to nitrogen ratio and many more [15, 20]. As a result, any sharp variation in these parameters could adversely affect the substrate concentration in the biodigesters. Some of the operating parameters are discussed in Sections 2.2.1–2.2.4.

#### 2.1.1.1 Organic loading rate (OLR)

This is generally expressed in terms of the amount of chemical oxygen demand (COD) or volatile solids (VS) of digester volume in a day and denoted as  $\text{KgCOD/m}^3 \text{ d}$  or  $\text{KgVS/dm}^3 \text{ d}$ . Most favourable COD removal of the canning industry effluent was found to be between 89 and 93% at OLRs of 9.8 and  $10.95 \text{ kgCOD/m}^3 \text{ d}$  at an HRT of 10 h at a pH of 5.5 [15, 18, 19]. This prediction becomes viable during the selection of the reactor-type and other process parameters such as pH control. OLR has been found to increase with decreasing biodegradation of the volatile solid and the subsequent bioenergy produced. The performances of bioreactors decrease when the OLRs increase with energy production [10, 15, 17].

Furthermore, the pH range suitable for AD is reported to be within the range of 6.8–7.2 [13]. This is achieved by charging the AD at an optimum OLR to obtain a higher yield of biogas. There is usually a variation in pH during AD especially during acidogenesis where volatile fatty acids such as propionate, butyrate and acetates are produced [19]. The presence of phosphates ( $\text{PO}_4^-$ ) in most wastewater treatment facilities renders the pH adjustment with calcium hydroxide possible to a pH of about 7.2, even at high concentrations. The growth of microorganisms in AD is largely dependent on the pH of the substrates undergoing the overall biodegradation [8]. In the treatment of wastewaters, the observed pH range of 6.0–7.1 was been reported in a study where a mixed batch reactor produced larger quantities of biogas at an average value of  $0.405 \text{ m}^3/\text{d}$  [11].

#### 2.1.1.2 Temperature

Temperature conditions during the AD process for bioenergy production includes psychrophilic ( $<30^\circ\text{C}$ ), mesophilic ( $30\text{--}40^\circ\text{C}$ ) and thermophilic ( $50\text{--}60^\circ\text{C}$ ) [8, 12]. The anaerobes are found to be more active under both mesophilic and thermophilic temperatures as compared to psychrophilic temperatures. Comparatively, thermophilic temperatures are considered suitable for the enhancement of biomethanation by accelerating the hydrolysis of the polymeric feedstock and other metabolic pathways [12, 13]. However, several studies have shown that thermophilic digesters suffer from poor process stability due to volatile fatty acid accumulation during the acidogenesis process, most especially propionate [13, 17].

#### 2.1.1.3 Hydraulic retention time (HRT)

This is the measure of the time required to achieve the complete biodegradation of an organic matter associated with process parameters such as the temperature of the medium and the waste composition [12]. The HRTs observed in AD under mesophilic and thermophilic temperatures are 15–30 days and 12–14 days respectively [13, 17]. Temperature and HRT effects on the methanogenesis process have been observed in a study by Shah et al. [13]. In the same study, the working temperature was adjusted from 30 to  $55^\circ\text{C}$  following an HRT of 8–12 days.

### 2.1.2 Applications of the anaerobic digestion process

The full-scale application of the AD technique in the treatment of industrial wastewater depends on the hydrodynamic configuration of the AD reactor. There have been different types of AD reactors applicable in the wastewater treatment settings, which includes continuous stirred tank reactor (CSTR), the anaerobic sequencing batch reactor (ASBR), upflow hybrid anaerobic sludge-filter bed (UASFB), upflow anaerobic sludge blanket reactor (UASBR), expanded granular sludge bed (EGSB), anaerobic baffled reactor (ABR), anaerobic fixed-bed reactors (AFBR) and integrated bio-membrane reactors [8, 13, 15–17]. For instance, **Figure 3** depicts schematic cross section view of the upflow hybrid anaerobic sludge-filter bed and the upflow anaerobic sludge blanket reactor. The integrated anaerobic-aerobic bioreactors have been most preferred in the past few decades due to its ability to meet stringent constraints in terms of mitigating odorant compound release and minimising sludge production.

#### 2.1.2.1 Limitations of adapting AD process in large scale

Research has shown that among the various reactors used in the performances for the treatment of wastewaters, the UASBR configuration is the most widely used with a high-rate anaerobic reactor for the treatment of high-strength wastewater [8, 12]. Several modifications have been carried out in the design of bioreactors to enhance both the consistency and the efficiency of the reactors. The AD process does encounter failures causing serious environmental hazards [8]. In addition, some of the aforementioned operating parameters as previously discussed (Section 2.2) can affect the performances of the microbes responsible for the biodegradation of organic matter in the wastewater settings. Further drawbacks observed in AD large scale operation include microbial shift, process instability, low yield of biogas production and poor water quality [8, 10, 12, 14, 19]. For instance, monodigestion of energy crops still struggle to meet the reduction targets concerned with the drawbacks in AD compared to anaerobic co-digestion (AcoD) such as a mixture of slurry and energy crops [5, 20]. In response, pretreatment techniques for cellulose enhancement and the use of energy crops as feed stocks have been found to increase the efficacy of biogas production via AD [12]. Some of the improvement techniques which have gained attention in terms of research for the betterment of AD process design and the optimisation includes

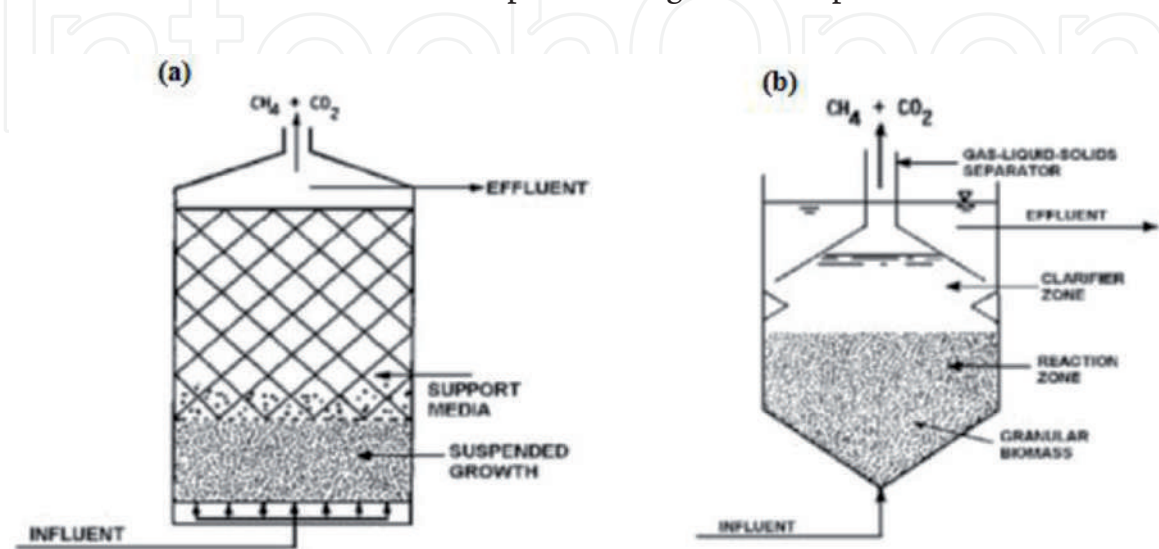


**Figure 3.**  
(a) Upflow-hybrid anaerobic sludge-filter bed and (b) upflow-anaerobic sludge blanket reactor [8].

evaluating the AD process kinetics and dynamics, nitrification-denitrification, recycling of the centrate back to the AD reactor, wastewater characterisation, optimisation of operational and environmental parameters, and microbial community shift.

### 2.1.3 Future prospects of AD application

According to the United Nations Sustainability Development Goal of 2030, the use of renewable energy is expected to reach 100% by the year 2050. The seventh goal focuses on the production of affordable and clean energy globally which is environmentally friendly [21, 22]. Renewable energy has gained attention to cater for the ever-increasing use and over-reliance of non-renewable forms of energy. This arises because of the emission of greenhouse gases compelling researchers in the past decades to search for an alternative means of sustainable energy production [17, 23–25]. The reserve for energy has become necessary for global concern in maintaining a sustainable way in lieu of the resources available especially at WWTPs. Aside the protection of the environment, wastewater treatment plants (WWTPs) also serve as a source of generating renewable forms of energy such as biogas. In a WWTP, the dumping of sewage sludge produced as a by-product is a problem of growing significance representing up to 50% of the entire operating costs of all WWTPs [8, 12, 14]. Also, wastewaters with a high content of nitrogen can be treated with the nitrification and denitrification technique form of AD generally known as Anammox [26]. Constructive government policies have shown Germany as being the dominant global biogas energy generation country globally for the future [23, 25]. Latest reports predict that biogas production could increase from 18,244 Gigawatt hours (GWh) in 2012 to 28,265 GWh in 2025, indicating a compound annual growth rate (CAGR) of 3.4%. In 2011, Germany contributed the largest share of the world's cumulative installed capacity as the country accounted for approximately a quarter of the global biogas biogas [23, 25, 27].

## 3. Membrane technology

Membranes, as a thin layer barrier for size differential separation, are usually integrated with chemical and biological treatment or standalone systems in secondary treatment of wastewater settings [28–30]. In a typical membrane mechanism, there is usually a driving force, such as a semi-permeable barrier which controls the rate of movement of components by fractional permeation and rejection through pores of different sizes as depicted in **Figure 4** [32]. The permeation and selective rejection is a function of the membrane pore size and chemical affinity, which helps

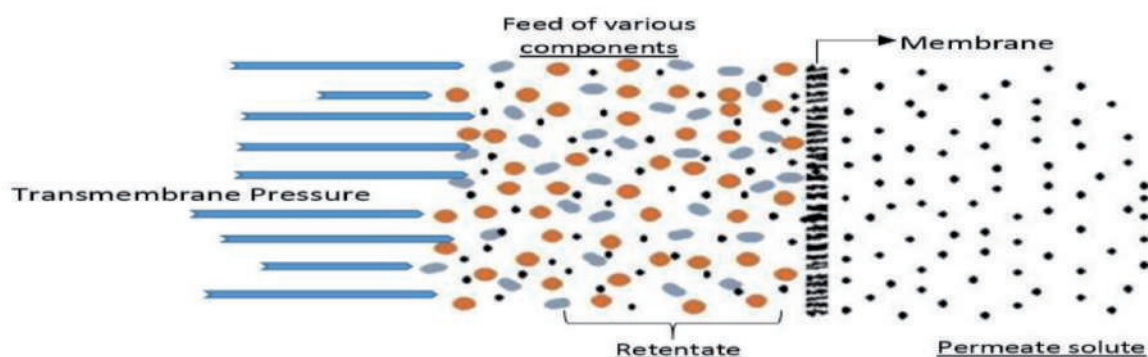


**Figure 4.** Membrane selective permeation for various solutes adapted from [31].

to have a product stream devoid of target components [33]. Due to the relatively low energy requirement and wastewater treatability efficiency, membrane technology has tremendously improved by the development of new materials and configurations for industrial applications. Some of these applications include microbial fuel cells, removal of organic and inorganic components, disinfection, pathogen removal and desalination [30, 33, 34].

### 3.1 Types of membrane technologies

Generally, the major driving force for selective filtration is a potential gradient of variables such as hydrostatic pressure, electrical voltage, temperature, concentration or a combination of these driving forces [29, 32]. These variables including nature (natural and synthetic) and structure (porous or non-porous and heterogeneous or homogenous) have been used in the classification of membranes [28, 31, 32, 34]. However, most commercially available and industrially used membranes are pressure-driven and energy driven (electrodialysis and electrodialysis reversal) membranes [35]. Pressure driven types are namely microfiltration (MF), ultrafiltration (UF), reverse osmosis (RO) and nanofiltration (NF). These are also classified by their pore sizes or molecular weight cut-off (MWCO). MWCO is expressed in Daltons ( $1 \text{ Da} = 1 \text{ g mol}^{-1}$ ) and is the minimum or smallest component that can be retained with at least 90% efficiency [28, 30, 32, 35]. It should be noted that as the pore size of these membranes decrease, the driving force for the operation increases. For instance, the MF and UF are referred as low pressure driven processes while RO and NF are high pressure driven processes [28, 29, 34].

### 3.2 Applications of membrane technology

#### 3.2.1 Microfiltration (MF) application

Microfiltration utilises a sieving mechanism to retain macromolecules or particles more than  $0.1 \mu\text{m}$ , specifically in the range of  $0.1\text{--}10 \mu\text{m}$  [30]. Unlike UF, RO and NF, the transmembrane pressure (TMP) for both sides of the membrane as a result of the small particle retention is puny, hence requiring a relatively small TMP lower than 2 bar but varies from 0.1 to 2 bar [28, 30]. As indicated, the larger pore sizes of MF membranes limit removal to suspended solids, bacteria, some viruses (up to 2-log), protozoan cyst, turbidity and on a lesser extent, organic colloids within the region [28, 29, 32].

#### 3.2.2 Ultrafiltration (UF) application

The role of UF is increasing as a pretreatment for desalination and membrane bioreactors. Ultrafiltration (UF) like MF utilises physical sieving as a separation mechanism. The pore size, MWCO and pressure for a UF membrane ranges from  $0.05 \mu\text{m}$  to  $1 \text{ nm}$ ,  $1\text{--}500 \text{ kDa}$  and operating pressure of  $1\text{--}7 \text{ bar}$  [30, 33]. As such, UF with a definite MWCO are impermeable to compounds with molecular weights exceeding the MWCO and have shown a 3–6 log removal of chlorine resistant protozoan cysts, active *Giardia lamblia*, colloids, viruses and coliform bacteria. The use of MF and UF as pretreatment to RO has gradually emerged as an industry standard. Both are often used as pretreatment for NF and RO processes to reduce membrane fouling and is also applied as a post treatment to chemical precipitation for organic chemical removal and pH adjustment, phosphorus, hardness and metals [29–31, 33, 34]. Fouling is highly eminent in UF due to the high molecular weight of fractions retained in relations with the small osmotic pressure differentials and

liquid phase diffusivity. However, this does not negatively influence the demand for UF's as any design, configuration and application will be fouled [28, 30, 36]. The configuration for application is influenced by the mechanical stability, hydrodynamic requirement and economic limitations.

### 3.2.3 Nanofiltration (NF) application

Nano filtration is a pressure related process where the mechanism of separation is based on molecular size for the removal of dissolved micro pollutants and multivalent ions. The NF is a complex process characterised by solvent diffusion, transport and electrostatic repulsion effects at the membrane surface and within the nanopores [29, 30]. The difference between the pore diameter and particle size forms the basis of the sieve effect. Based on the membrane pore size, NF is often referred to as 'loose RO' with separation taking place at the lower end of UF and upper end of RO as it covers a MWCO of 100–500 Da, a pore size of 0.5–5 nm and operates at relatively low pressure of 5–35 bar [28, 30, 34]. The NF is usually deployed in the removal of polyvalent cation, reduction in colour, tannins, turbidity and disinfection by-product precursors such as organic matter as their potency lies in the high rejection of divalent ions (98%), permeation of monovalent ions (20–80% rejection) and high flux. Nano filtration is often used as a post treatment or polishing step in conventional treatment processes. Although it is not advisable to be used in desalination processes, it is used to reduce the salt content of slightly saline water. Recent applications have used NF as a pretreatment to RO reducing the operating pressure in RO providing savings in operational and maintenance costs [31, 32, 35]. Second stage fouling is usually reduced in NF systems through ozone pretreatment and non-thermal crystallisation while cleaning is done using suitable alternatives that also exist for MF and UF [30, 33].

### 3.2.4. Reverse and forward osmosis

Reverse osmosis, often referred to as tight membrane has been widely used in brackish water and wastewater treatment with its effectiveness in desalination against conventional thermal Multi stage flash. High external pressure of 15–150 bar which is a function of the hypertonic feed and greater than the osmotic pressure is applied to retain dissolved solute and solvent permeation at a MWCO around 100 Da through diffusion mechanism [37–39]. Using concentration gradient as the driving force, separation and concentration in forward osmosis (FO) occurs as the concentrated solution (e.g., salts such as NaCl) draws water from a less concentrated feed solution. Characteristic advantages include low energy consumption, simple configuration and operation, low membrane fouling tendency and high rejection of a wide range of contaminants. The use of FO operates at ambient conditions, hence irreversible fouling is low [37, 39]. However, FO technology is faced with the lack of recyclable and economical drawing solutions, internal and external concentration polarisation and a difficulty of developing effective large scale plants [37]. To achieve desired process flow and optimum configuration, ROs are arranged in stages and passes. The sequence of the stages has the concentrate stream of the first stage as the feed inlet of the second stage. Permeate streams from both streams are summed into one discharge channel. However, passes involve either a one path recovery of permeate or the rechanneling of permeates from the first RO into the second RO to improve quality [40, 41] as summarised in **Table 1**.

Membrane	Microfiltration	Ultrafiltration	Nanofiltration	Reverse osmosis
Structure	Asymmetrical (thickness 10–150 $\mu\text{m}$ )	Symmetric (thickness = 10–200 $\mu\text{m}$ ) or asymmetric (thickness = 0.1–0.5 $\mu\text{m}$ and supported by sublayer of 50–150 $\mu\text{m}$ )	Asymmetric 150 $\mu\text{m}$	Asymmetric 150 $\mu\text{m}$
Material	Ceramic, PP, PSO, PVDF	Ceramic, PTFE, PSO, CA, PVDF, thin film	PA, CA, PES, SPSF, PI, PVA, CS, organic/inorganic hybrids: thin film	Zeolite, PVDF, PES, PBI, TFC
Transport Laws	Darcy's Law	Darcy	Fick's	Fick's
Module	Dead end: flat sheet or spiral wound Cross flow: capillary, hollow fibre or tubular	Capillary, spiral wound, others: tubular, plate and frame, rotary modules, vibrating modules and dean vortices	Tubular, spiral wound, plate and frame	Tubular, spiral wound, plate and frame
Configuration	Dead end, cross flow, transverse flow	Dead end, cross flow, transverse	Shell-side feed, bore-side feed, cross flow	Cross flow in various stages and passes

*PBI, polybenzimidazole; CA, cellulose acetate; PSO, polysulfone; PP, polypropylene; PVDF, polyvinylidene fluoride; PES, polyethersulfone; TFC, thin film composite.*

**Table 1.**  
 Summary of pressure-driven membranes [39–41].

### 3.2.5 Membrane bioreactors

Low-pressure driven MF and UF used for critical solid-liquid separation has been integrated with biological treatment into a hybrid activated sludge process termed as membrane bioreactors (MBR) for wastewater treatment. Unlike conventional wastewater treatment processes with treatment limitations, MBRs have shown wide range treatment efficiency in the removal of organic and inorganic emerging micro pollutants including pesticides, antibiotics, analgesics, anti-epileptic, biodegradable organic compounds, microplastics, industrial chemicals and nutrients [30, 42, 43]. The MBRs can be configured into gravity or submerged vacuum driven systems by using hollow fibre or flat sheet modules, while pressure driven membranes on the other hand are mostly configured with external pipe cartridge systems. The MBR is usually combined with conventional systems including thermophilic or mesophilic bioprocesses, AOPs, powdered activation carbon to enhance improve the water quality and treatability efficiency [39, 40, 42, 44]. Some of the advantages of MBRs include small foot-print requirement, simple transport configuration and the ability to handle high biomass concentrations [45].

### 3.2.6 Ion exchange membrane

Ion exchange membranes are classified as anion exchange membrane (AEM) if the polymer matrix is embedded with fixed positive charge groups and vice

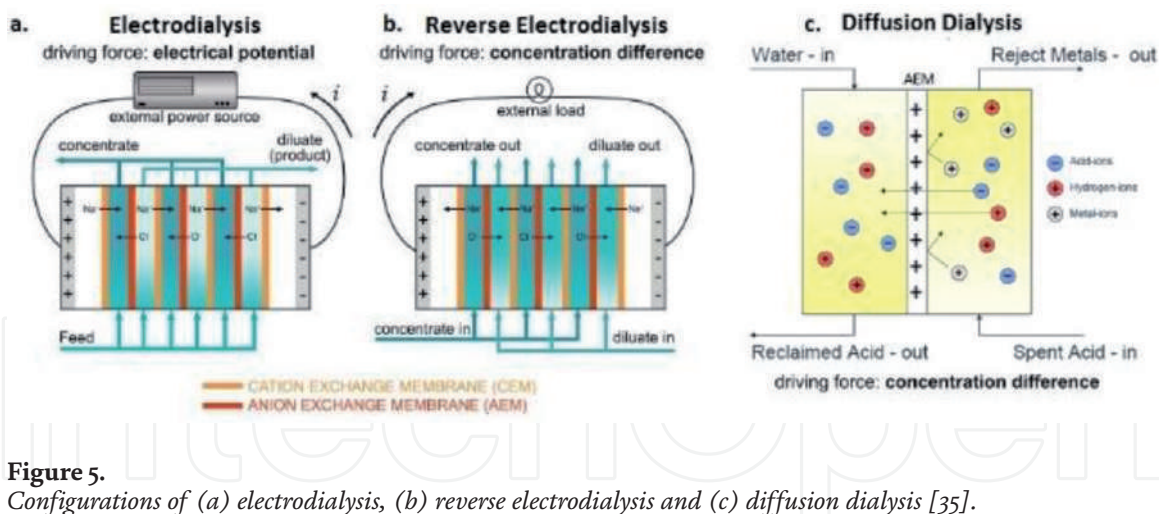


Figure 5.

Configurations of (a) electro dialysis, (b) reverse electro dialysis and (c) diffusion dialysis [35].

versa for cation exchange membranes (CEM) [35]. This involves the permeation of anions/cations and rejection of cations/anions in the effluent. Electro dialysis (ED), reverse electro dialysis (RED), diffusion dialysis (DD) and Donnan membrane process (DMP) are examples of these, which usually involves the exchange of ions between the solutions across the membrane as shown in **Figure 5**. The application of these processes is usually based on the type of effluent and is reported to be non-fouled and energy resourceful as mechanism of separation is by potential gradient. The DD is applied to reclaim free mineral acids and alkalis while DMP is used in recovery of toxic and valuable metals from various feeds. In both DD and DMP, a Donnan equilibrium is established hence their difference lies in application areas. Unlike ED and RED, DD and DMP are being applied on bench scale, have osmotic limitations and therefore kinetic studies are being considered for various effluents. However, ED and RED constructions requires compatibility of feed stream and stack materials, electrical safety consideration and larger footprint to produce equivalent water quantity and quality [30, 32, 33, 36].

#### 4. Advanced oxidation process

Basically, there are two stages which are usually employed in wastewater treatment settings via a pre-treatment step involving mechanical and physicochemical systems to reduce the heterogeneous components of the effluents followed by an advanced treatment process. The physicochemical process enhances the efficiency of the advanced treatment by agglomerating the containments into a larger size for easy filtration or removal [46, 47]. However, degradation of emerging recalcitrant components with membrane and bioremediation in advanced treatment processes attests to be complex. So, in addressing this problem, advanced oxidation process (AOP) has gained much attention due to its potential to degrade a wide range of organic micro-pollutants [47, 48]. This process involves the generating of potent reactive hydroxyl radicals ( $E_0 = 2.8 \text{ eV}$ ) with photon energy and without further additional chemical treatment. Examples are chemical oxidation ( $\text{O}_3$ , Fenton reagents), photochemical oxidation (Ultraviolet-UV/ $\text{O}_3$ , UV/ $\text{H}_2\text{O}_2$ ), heterogeneous photocatalysis (UV/ $\text{TiO}_2$ ), electrolysis and sonolysis [46, 49–52] as shown **Figure 6**. These technologies use UV-A with long wavelengths of 315–400 nm, and UV-C with short wavelength radiation of 100–280 nm for degradation of most environmental contaminants. Generally, UV/ $\text{O}_3$  and UV/ $\text{H}_2\text{O}_2$  processes consume large amounts of oxidant, which makes them uneconomical to operate [43]. On the other hand,

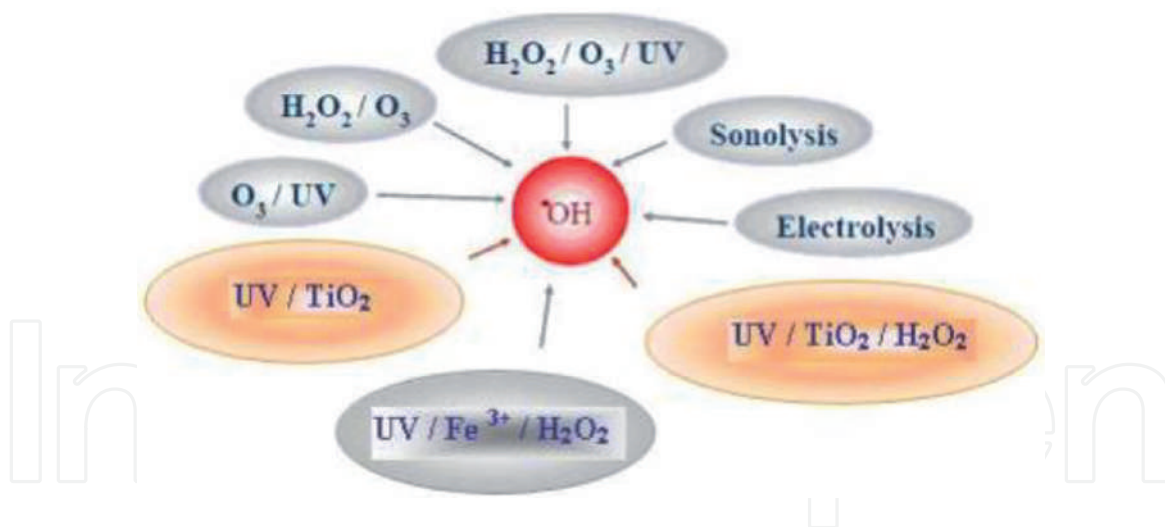


**Figure 6.**  
*Types of advance oxidation process (AOPs) adapted from [46].*

the hazards associated with ozone being an unstable gas limits its application and is usually coupled with an ozone-water contacting device to convert the ozone into its liquid phase thus increasing the cost of production. However, the considerable operational conditions of ambient temperature and pressure and the use of a low-cost and chemical stable catalyst ( $\text{TiO}_2$ ) are predominantly attractive for complete mineralisation of contaminants and by-products. This makes heterogeneous photocatalysis techniques to be advantageous over other AOP's. Other advantages include no sludge production, quick reaction rate, low cost and operating well at ambient temperature and pressure conditions [46, 49].

#### 4.1 Photocatalysis

There are several semiconductors favourable for water treatment such as  $\text{TiO}_2$ ,  $\text{ZnO}$ ,  $\text{Fe}_2\text{O}_3$ ,  $\text{CdS}$  and  $\text{ZnS}$ , which are active within a band gap energy of 2.3–3.2 eV and wave length of 413–539 nm [53, 54].  $\text{TiO}_2$  has been the most widely used photocatalyst and exists in three major crystalline polymorphs such as anatase, rutile and brookite (**Figure 7**). There have been intensive studies to determine the crystalline structure, surface area, density of surface hydroxyl groups and adsorption/desorption characteristics of  $\text{TiO}_2$  [46, 49]. As mentioned, the surface hydroxyl group concentration has been documented to play a vital role in the photocatalytic degradation process, such that an increase in concentration of the hydroxyl groups on the catalyst surface might have a positive effect on the reaction rate [46, 49, 51]. Thus, the hydroxyl radicals produced ( $\text{OH}^\cdot$ ) are a very combative species and are therefore able to oxidise a wide range of organic pollutants in a swift and effectual means.

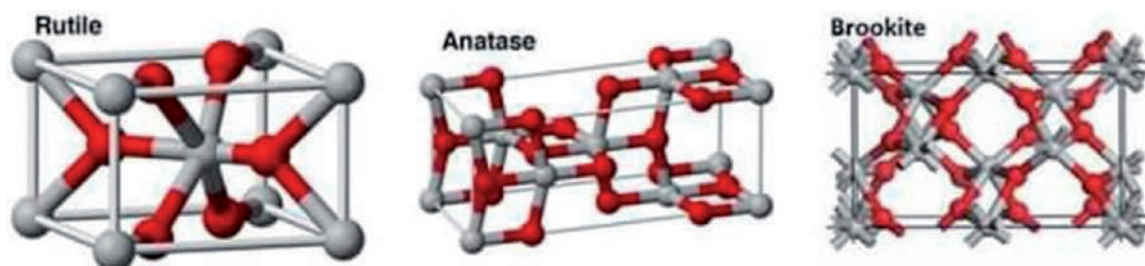


**Figure 7.**  
*Crystal structures of  $\text{TiO}_2$  adapted from [51, 52, 55].*

#### 4.1.1 Principles of heterogeneous photocatalysis

The heterogeneous photocatalysis process involves series of reactions such as oxidation, dehydrogenation, hydrogen transfer and metal deposition, among others [55]. Besides, the normal thermal and chemical catalytic actions that ease any distinctive chemical reaction require simultaneous activation of the molecules. As such, in photocatalysis, a light source with energy equal to or higher than the band-gap energy of the catalyst is employed to stimulate the catalyst to be active during the reaction bringing about the reduction or oxidation of the adsorbed species on the surface, for instance, oxidation of organic compounds into their subordinates until carbon dioxide and water are formed [56, 57]. This results in charge separation as the electron ( $e^-$ ) moves from the valence band to the conduction band of the semiconductor catalyst, resulting in a hole ( $h^+$ ) in the valence band as shown in **Figure 8**.

##### 4.1.1.1 Selection of catalysts

Some of the parameters to consider in selecting a photocatalyst to enhance the degradation capacity include the nature and intensity of light source, the amount of photons to activate the catalyst, the reaction medium and the water chemistry to generate the hydroxyl radicals, and the nature and concentration of the pollutants [46, 51, 55]. However, the relationship between the energy levels of conduction and valence bands with respect to the energy for reduction and oxidation is one of the cardinal points to consider in selecting a photocatalyst [46, 47]. The chemical capacity of the photo-generated electrons and holes has high influence on the conduction band energy level of the photocatalyst. Thus the photo-generated electron of a catalyst should be able to

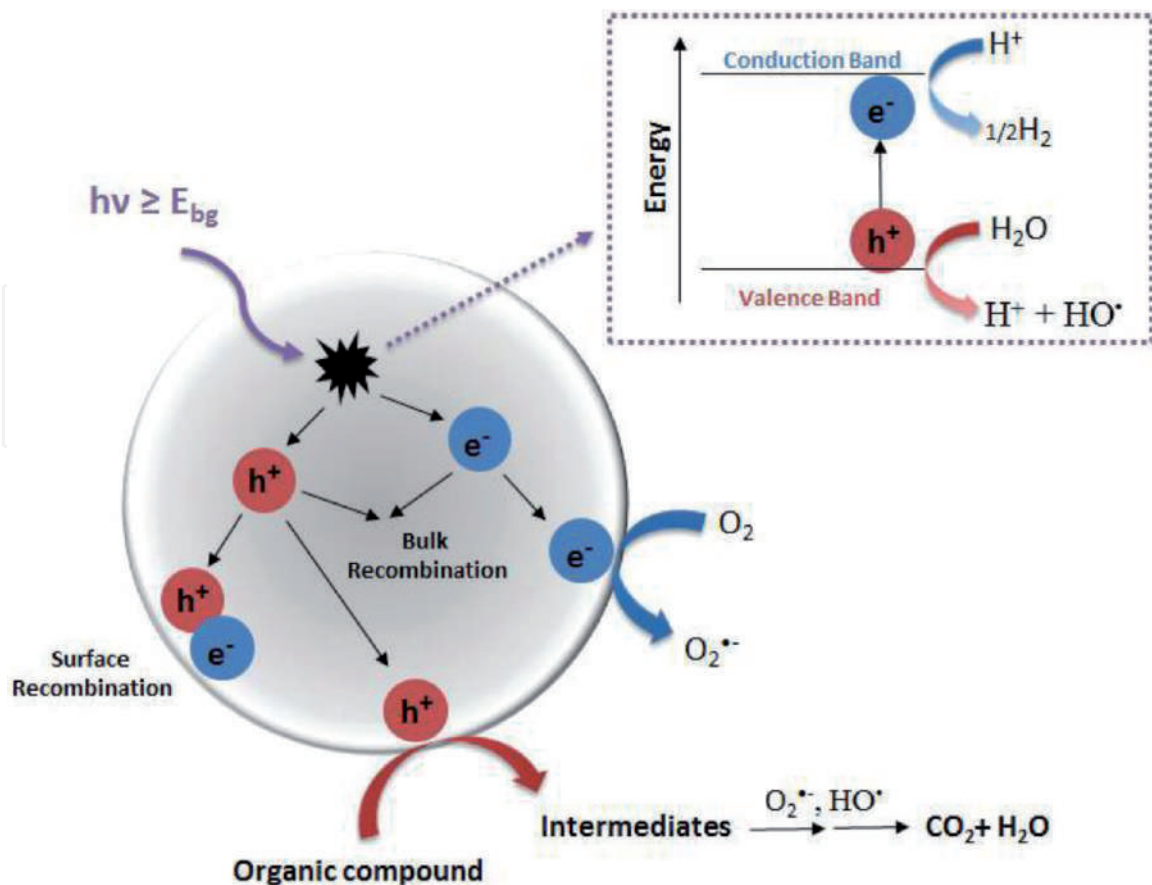


**Figure 8.** Schematic illustration of the photocatalytic mechanism in the presence of a water contaminant adapted from [46, 49, 52].

have essential energy to ease the mineralisation of the micro pollutants. The conduction band energy level of the photocatalyst in terms of mineralisation has to be more negative, while the valence band has to be more positive with respect to the energy for oxidation of water. This makes semiconductors with large band gaps to be considered as suitable for photocatalytic activities [46, 47, 50]. Thus, semiconductor materials are able to provide adequate negative and positive redox potentials in conduction bands and valence bands, respectively. In addition, the wider the band-gap of semiconductor material the higher the energy input to enhance its efficiency. Furthermore, the poor photo-corrosion stability of many semiconductors limits significantly the number of potential photo-catalytic materials for mineralisation in wastewater settings [55, 57].

#### *4.1.1.2 Modification of catalyst*

Photocatalytic activity of a distinctive semiconductor, such as  $\text{TiO}_2$ , can attract light energy equivalent to or higher than the band gap energy, resulting in generating electrons and holes. This electron-hole pair then migrates to the  $\text{TiO}_2$  surface and amalgamates with the adsorbed reactants to hasten the reduction and oxidation process. The lack of such an energy transfer leads to recombination of the pairs, which then competes with the desirable redox process with a high loss of energy. Therefore, to increase photocatalysis efficiency, suitable modification of the semiconductor band gap is essential to attract the recombination charge carriers which might hinder the photocatalytic efficiency. Some of these processes include (i) doping with metal cations and anions, (ii) coupling with other semiconducting oxides, (iii) sensitization with light harvesting compounds/dye molecules and (iv) plasmon resonance induced by specific metals [49, 51].

#### *4.1.2 Parameters affecting photocatalysis*

As with most processing techniques, several parameters affect the performance of the photocatalytic degradation process. Photocatalytic activities are being influenced by experimental conditions such as the amount of catalyst, light intensity, lighting area, reactor volume, pH type of reactor, temperature and pressure. Likewise, the inherent structural and properties of semiconductor photocatalyst influences its performance. This includes the particle size, phase composition, surface area, surface hydroxyls, lattice defects and the type of dopants (metals and non-metals) [46–48, 52]. The amount of light radiation absorbed is the driving force for semiconductor with threshold wavelength to provide the appropriate photon energy to overcome the band gap between the valence and conduction bands. This threshold wavelength is very important to promote electrons to be in an excited state corresponding to the band gap energy as depicted in **Table 2**.

#### *4.1.3 Applications of photocatalysis*

With the current greenhouse emission problems and energy deprivation situation, photocatalysis emerges as one of the alternative ways of providing feasible solutions to the global front in relation to energy and the environment. For instance (**Figure 9**), in the phenomenon of photosynthesis, green plants trap the solar energy from the sunlight and with a series of enzyme catalysed redox processes, converts the  $\text{CO}_2$  into water and carbohydrates by releasing oxygen into the atmosphere where most living organisms depend on to survive. In this scenario, photocatalysis which works with the same principle has gained incredible status and hence can be explored for divert applications in seeking sustainable energy, social economic growth and environmental impact.

Semiconductor	Band gap energy (eV)	Wavelength (nm)
TiO <sub>2</sub> (rutile)	3	413
TiO <sub>2</sub> (anatase)	3.2	388
ZnO	3.2	388
ZnS	3.6	335
CdS	2.4	516
Fe <sub>2</sub> O <sub>3</sub>	2.3	539

Adapted from [47].

**Table 2.**  
Semiconductors and their band gaps at specific wavelengths.

#### 4.1.3.1 Photocatalytic degradation in wastewater

The importance of photocatalytic degradation technology in pre- and post-treatment of water and wastewater using sunlight on a large scale is at the verge of development, with few of them like self-cleaning, anti-fogging and anti-bacterial applications currently being practiced. For instance, two slurry reactors coupled with TiO<sub>2</sub> were built in New Mexico (USA) and Almeria (Spain); however, the environmental conditions, low photonic yield and efficiency under the visible light make it challenging to be commercialised [27, 60–63]. There are numerous studies ongoing seeking to address some of these limitations in order to improve the photocatalyst, reactor design and light efficiency [55, 59]. Furthermore, the kinetics study to understand the mechanistic pathways of mineralisation of recalcitrant organic and micropollutants has also received attention.

#### 4.1.3.2 Photocatalytic energy production

In the early 1900s, the photocatalytic techniques commonly referred to as “artificial photo-synthesis” was employed in reducing CO<sub>2</sub> into useful hydrocarbons (Figure 9). This has now attained incredible status on the global level. Currently researchers, scientists and engineers are exploring the mechanism to control the current atmospheric carbon dioxide levels (green-house gas effect) by altering it into fuels and useful chemicals, and the role of CO<sub>2</sub> as a source of energy. However, the

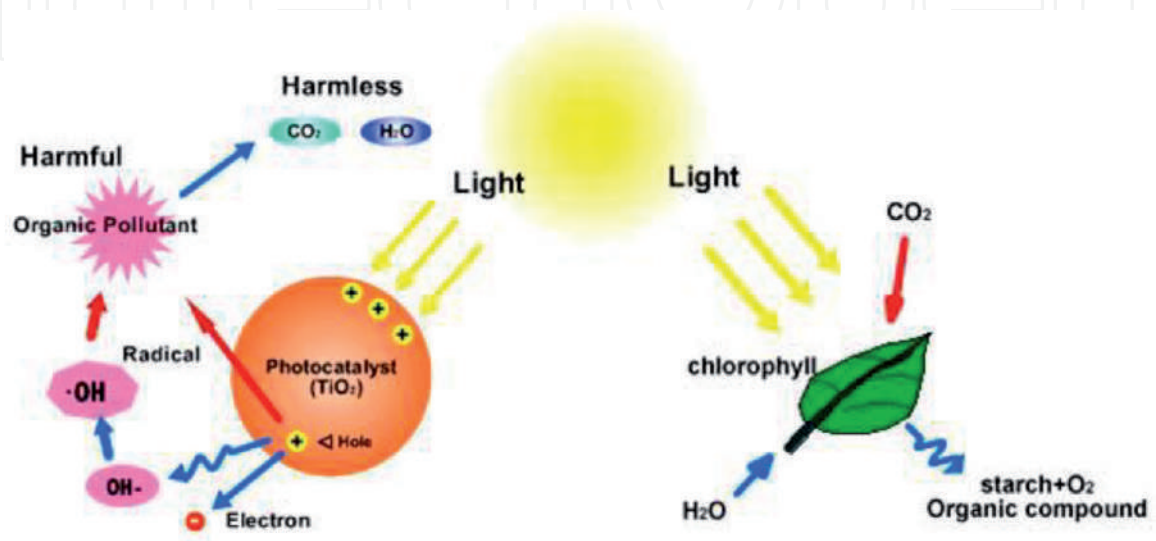


**Figure 9.**  
Schematic comparison of photo-catalysis and photo-synthesis [58, 59].

use of solar energy via chemical storage can be attained by photocatalytic or photo-electrochemical initiation of light-sensitive catalytic surfaces. Due to the simplicity of the photocatalytic process, it can be employed in converting solar energy into other useful forms of energy like hydrogen via splitting of water and hydrocarbons (methane, methanol, etc.), commonly known as solar fuels [52, 55, 59].

#### *4.1.4 Future prospects for photocatalysis*

There have been tremendous efforts dedicated to improving photocatalytic degradation efficiency, where some role of the aforementioned parameters on the AOPs performance have been studied with different types of wastewaters from the textile, oil refinery, slaughterhouses [46, 47, 59]. However, in relation to relative operational and energy utilisation costs, as well as the formation of unknown toxic intermediates from the parent compounds (semiconductors) and the pollutants remain unsolved. Although, this method is prone to shifting of hydroxyl radicals by non-target substances, but some are not suitable for certain varieties of toxic compounds that can counterattack the hydroxyl radicals rendering an increase in ecotoxicity when discharged into the environment. In response, there have been attempts to improve the semiconductor material performance by discovering the reaction mechanisms to develop commercial scale technology, but there are still some challenges which include mass transfer limitations, catalyst deactivation, generation of intermediate products and by-products, and the multi-complex optimisation of the materials and the reactor configuration [49, 55, 58]. Furthermore, due to the intrinsic nature of photocatalysis, it is very difficult to model photocatalytic reactors with a uniform light along the whole reactor volume [58, 59]. Therefore, a feasibility study on the irradiance distribution inside the reactor is required, especially with heterogeneous media such as TiO<sub>2</sub> in suspension.

## **5. Conclusion**

The availability of a cost effective technology to ensure the economic viability of wastewater settings for domestic and industrial purposes is still limited. This chapter presented the insights in applicability of some of the cost-effective technologies in addressing the global water, energy and environmental concerns. The fate of biological systems (AD process), and some of its operating parameters essential for wastewater treatment and bioremediation to energy (biogas) were also discussed. Furthermore, limitations, applications and different configuration types of AD reactors, as well as the forthcoming of the AD process as the alternative technology for bioenergy production using wastewater as a source was discussed. The emerging membrane technologies such as Donnan membrane process are also spotted as the foreseen green and energy saving technologies for industrial and environmental applications. The future challenge for using AOPs in wastewater treatment could be addressed by developing a cost effective photocatalyst to enhance the wastewater treatment and coupled in reduction of carbon dioxide as a renewable energy source to fuels. Therefore, adapting strategies for processes integration and commercialisation of the aforementioned technologies will enhance sustainable social economy growth and development.

## **Acknowledgements**

The authors wish to thank Durban University of Technology, National Research Foundation and Water Research Commission, South Africa, for their support.

IntechOpen

IntechOpen

### Author details

Emmanuel Kweinor Tetteh\*, Sudesh Rathilal, Maggie Chetty,  
Edward Kwaku Armah and Dennis Asante-Sackey  
Department of Chemical Engineering, Faculty of Engineering and the Built  
Environment, Durban University of Technology, Durban, South Africa

\*Address all correspondence to: [ektetteh34@gmail.com](mailto:ektetteh34@gmail.com)

### IntechOpen

---

© 2019 The Author(s). Licensee IntechOpen. This chapter is distributed under the terms of the Creative Commons Attribution License (<http://creativecommons.org/licenses/by/3.0>), which permits unrestricted use, distribution, and reproduction in any medium, provided the original work is properly cited. 

## References

- [1] De Andrade JR, Oliveira MF, Da Silva MGC, Vieira MGA. Adsorption of pharmaceuticals from water and wastewater using nonconventional low-cost materials: A review. *Industrial and Engineering Chemistry Research*. 2018;**57**(9):3103-3127
- [2] Freyria F, Geobaldo F, Bonelli B. Nanomaterials for the abatement of pharmaceuticals and personal care products from wastewater. *Applied Sciences*. 2018;**8**(2):170
- [3] Carlos FS, Schaffer N, Andreazza R, Morris LA, Tedesco MJ, Boechat CL, et al. Treated industrial wastewater effects on chemical constitution maize biomass, physicochemical soil properties, and economic balance. *Communications in Soil Science and Plant Analysis*. 2018;**49**(3):319-333
- [4] Rincón Llorente B, De la Lama-Calvente D, Fernández-Rodríguez MJ, Borja-Padilla R. Table olive wastewater: Problem, treatments and future strategy. A review. *Frontiers in Microbiology*. 2018;**9**:1641
- [5] Abbas A, Valek L, Schneider I, Bollmann A, Knopp G, Seitz W, et al. Ecotoxicological impacts of surface water and wastewater from conventional and advanced treatment technologies on brood size, larval length, and cytochrome P450 (3A3) expression in *Caenorhabditis elegans*. *Environmental Science and Pollution Research*. 2018;**25**(14):13868-13880
- [6] Tetteh EK, Rathilal S. Effects of a polymeric organic coagulant for industrial mineral oil wastewater treatment using response surface methodology (Rsm). *Water SA*. 2018;**44**(2):155-161
- [7] Dohare D, Meshram R. Biological treatment of edible oil refinery wastewater activated sludge process and sequencing batch reactors—A review. *International Journal of Engineering Sciences & Research Technology*. 2014;**3**(12):251-260
- [8] Chan YJ, Chong MF, Law CL, Hassell DG. A review on anaerobic-aerobic treatment of industrial and municipal wastewater. *Chemical Engineering Journal*. 2009;**155**(1-2):1-8
- [9] Patil JH, AntonyRaj MA, Shankar BB, Shetty MK, Kumar BP. Anaerobic co-digestion of water hyacinth and sheep waste. *Energy Procedia*. 2014;**52**:572-578
- [10] Tetteh E, Amano KOA, Asante-Sackey D, Armah EKA. Response surface optimisation of biogas potential in co-digestion of miscanthus fuscus and cow dung. *International Journal of Technology*. 2018;**9**(5):944-954
- [11] Kougiaris PG, Angelidaki I. Biogas and its opportunities—A review. *Frontiers of Environmental Science & Engineering*. 2018;**12**:1-2
- [12] Appels L, Baeyens J, Degève J, Dewil R. Principles and potential of the anaerobic digestion of waste-activated sludge. *Progress in Energy and Combustion Science*. 2008;**34**(6):755-781
- [13] Shah FA, Mahmood Q, Rashid N, Pervez A, Raja IA, Shah MM. Co-digestion, pretreatment and digester design for enhanced methanogenesis. *Renewable and Sustainable Energy Reviews*. 2015;**42**:627-642
- [14] Sreekrishnan TR, Kohli S, Rana V. Enhancement of biogas production from solid substrates using different techniques—A review. *Bioresource Technology*. 2004;**95**(1):1-10
- [15] Kaparaju P, Serrano M, Angelidaki I. Optimization of biogas production from wheat straw stillage

in UASB reactor. *Applied Energy*. 2010;**87**(12):3779-3783

[16] Brito AG, Peixoto J, Oliveira JM, Oliveira JA, Costa C, Nogueira R, Rodrigues A. Brewery and winery wastewater treatment: Some focal points of design and operation. In: *Utilization of by-Products and Treatment of Waste in the Food Industry*. Boston, MA: Springer; 2007. pp. 109-131

[17] Achinas S, Achinas V, Euverink GJ. A technological overview of biogas production from biowaste. *Engineering*. 2017;**3**(3):299-307

[18] Chan YJ, Chong MF, Law CL. Performance and kinetic evaluation of an integrated anaerobic-aerobic bioreactor in the treatment of palm oil mill effluent. *Environmental Technology*. 2017;**38**(8):1005-1021

[19] Kainthola J, Kalamdhad AS, Goud VV. Optimization of methane production during anaerobic co-digestion of rice straw and hydrilla verticillata using response surface methodology. *Fuel*. 2019;**235**:92-99

[20] Aqaneghad M, Moussavi G. Electrochemically enhancement of the anaerobic baffled reactor performance as an appropriate technology for treatment of municipal wastewater in developing countries. *Sustainable Environment Research*. 2016;**26**(5):203-208

[21] Nilsson M, Griggs D, Visbeck M. Policy: Map the interactions between sustainable development goals. *Nature News*. 2016;**534**(7607):320

[22] Waage J, Yap C, Bell S, Levy C, Mace G, Pegram T, et al. Governing the UN sustainable development goals: Interactions, infrastructures, and institutions. *The Lancet Global Health*. 2015;**3**(5):e251-e252

[23] Tiwary A, Williams ID, Pant DC, Kishore VVN. Emerging perspectives

on environmental burden minimisation initiatives from anaerobic digestion technologies for community scale biomass valorisation. *Renewable and Sustainable Energy Reviews*. 2015;**42**:883-901

[24] De Besi M, McCormick K. Towards a bioeconomy in Europe: National, regional and industrial strategies. *Sustainability*. 2015;**7**(8):10461-10478

[25] Scarlat N, Dallemand JF, Fahl F. Biogas: Developments and perspectives in Europe. *Renewable Energy*. 2018;**129**:457-472

[26] Liu Y, Chen N, Liu Y, Liu H, Feng C, Li M. Simultaneous removal of nitrate and hydrogen sulfide by autotrophic denitrification in nitrate-contaminated water treatment. *Environmental Technology*. 2018:1-2

[27] Carley JK, Pasternack GB, Wyrick JR, Barker JR, Bratovich PM, Massa DA, Reedy GD, Johnson TR. Significant decadal channel change 58-67 years post-dam accounting for uncertainty in topographic change detection between contour maps and point cloud models. *Geomorphology*. 2012;**179**:71-88

[28] Warsinger DM et al. A review of polymeric membranes and processes for potable water reuse. *Progress in Polymer Science*. 2018;**81**:209-237

[29] Diallo MS. Water treatment by dendrimer-enhanced filtration: Principles and applications. In: *Nanotechnology Applications for Clean Water*. William Andrew Publishing; 2009. pp. 143-155

[30] Frenkel VS. Membranes in water and wastewater treatment. In: *Proceedings of the World Environmental and Water Resources Congress*. 2008. pp. 316-324

[31] Hamouda SB, Touati K, Amor MB. Donnan dialysis as membrane

process for nitrate removal from drinking water: Membrane structure effect. *Arabian Journal of Chemistry*. 2017;**10**:S287-S292

[32] Van Der Bruggen B. Integrated membrane separation processes for recycling of valuable wastewater streams: Nanofiltration, membrane distillation, and membrane crystallizers revisited. *Industrial and Engineering Chemistry Research*. Jan 2013;**52**(31):10335-10341

[33] Bodzek M. Membrane technologies for the removal of micropollutants in water treatment. In: *Advances in Membrane Technologies for Water Treatment: Materials, Processes and Applications*. Woodhead Publishing; 2015. pp. 465-517

[34] Shahmansouri A, Bellona C. Nanofiltration technology in water treatment and reuse: Applications and costs. *Water Science and Technology*. 1 Feb 2015;**71**(3):309-319

[35] Tedesco M, Hamelers HV, Biesheuvel PM. Nernst-Planck transport theory for (reverse) electro dialysis: II. Effect of water transport through ion-exchange membranes. *Journal of Membrane Science*. 2017;**531**:172-182

[36] Asante-Sackey L, Rathilal D, Tetteh S, Pillay EK. Optimization of donnan dialysis for alum recovery using box behnken design. In: *CBU International Conference Proceedings*. 2018. pp. 1007-1012

[37] Abdullah WN, Lau WJ, Aziz F, Emadzadeh D, Ismail AF. Performance of nanofiltration-like forward-osmosis membranes for aerobically treated palm oil mill effluent. *Chemical Engineering and Technology*. 2018;**41**(2):303-312

[38] Guo Y, Qi PS, Liu YZ. A review on advanced treatment of pharmaceutical wastewater. In: *IOP Conference Series: Earth and Environmental Science*. IOP Publishing; 2017;**63**(1):012025

[39] Mehta BB, Joshi RN, Raval HD. A novel ultra-low energy reverse osmosis membrane modified by chitosan with glutaraldehyde crosslinking. *Journal of Applied Polymer Science*. 2018;**135**(10):45971-45977

[40] Lin S, Elimelech M. Staged reverse osmosis operation: Configurations, energy efficiency, and application potential. *Desalination*. 2015;**366**:9-14

[41] Johnson J, Busch M. Engineering aspects of reverse osmosis module design. *Desalination and Water Treatment*. 2010;**15**(1-3):236-248

[42] Bodzek M, Konieczny K. Membranes in organic micropollutants removal. *Current Organic Chemistry*. 2018;**22**(11):1070-1102

[43] Dezotti M, Lippel G, Bassin JP. *Advanced Biological Processes for Wastewater Treatment: Emerging, Consolidated Technologies and Introduction to Molecular Techniques*. Springer; 2017

[44] Pachés M, Martínez-Guijarro R, González-Camejo J, Seco A, Barat R. Selecting the most suitable micro-algae species to treat the effluent from an anaerobic membrane bioreactor. *Environmental Technology*. 2018:1-10

[45] Roy D, Azais A, Benkaraache S, Drogui P, Tyagi RD. Composting leachate: Characterization, treatment, and future perspectives. *Reviews in Environmental Science and Biotechnology*. 2018

[46] Thiruvengkatachari R, Vigneswaran S, Moon IS. A review on UV/TiO<sub>2</sub> photocatalytic oxidation process. *Korean Journal of Chemical Engineering*. 2008;**25**(1):64-72

[47] Sievers M. Advanced oxidation processes. In: *Treatise on Water Science*. 2010;377-408

- [48] Bethi B, Sonawane SH, Bhanvase BA, Gumfekar SP. Nanomaterials-based advanced oxidation processes for wastewater treatment: A review. *Chemical Engineering and Processing Process Intensification*. 2016;**109**:178-189
- [49] Ameta S, Ameta R. *Advanced oxidation processes for wastewater treatment: Emerging green*. Chemical Technology. Academic Press; 2018
- [50] Thakur RS, Chaudhary R, Singh C. Fundamentals and applications of the photocatalytic treatment for the removal of industrial organic pollutants and effects of operational parameters: A review. *Journal of Renewable and Sustainable Energy*. 2010;**2**(4):042701
- [51] Demeestere K, Dewulf J, Van Langenhove H. Heterogeneous photocatalysis as an advanced oxidation process for the abatement of chlorinated, monocyclic aromatic and sulfurous volatile organic compounds in air: State of the art. *Critical Reviews in Environmental Science and Technology*. 2007;**37**(6):489-538
- [52] Khaki MR, Shafeeyan MS, Raman AA, Daud WMAW. Application of doped photocatalysts for organic pollutant degradation—A review. *Journal of Environmental Management*. 2017;**198**:78-94
- [53] Diya'Uddein BH, Daud WMAW, Abdul Aziz AR. Treatment technologies for petroleum refinery effluents: A review. *Process Safety and Environmental Protection*. 2011;**89**(2):95-105
- [54] Hasan DB, Abdul Aziz AR, Daud WMAW. Oxidative mineralisation of petroleum refinery effluent using Fenton-like process. *Chemical Engineering Research and Design*. 2012;**90**(2):298-307
- [55] Kim JR, Kan E. Heterogeneous photocatalytic degradation of sulfamethoxazole in water using a biochar-supported TiO<sub>2</sub> photocatalyst. *Journal of Environmental Management*. 2016;**180**:94-101
- [56] Gaya UI, Abdullah AH. Heterogeneous photocatalytic degradation of organic contaminants over titanium dioxide: A review of fundamentals, progress and problems. *Journal of Photochemistry and Photobiology C: Photochemistry Reviews*. 2008;**9**(1):1-2
- [57] Bhatkhande DS, Pangarkar VG, Beenackers AA. Photocatalytic degradation for environmental applications—A review. *Journal of Chemical Technology and Biotechnology: International Research in Process, Environmental & Clean Technology*; 2002;**77**(1):102-116
- [58] Zhang T, Lin W. Metal-organic frameworks for artificial photosynthesis and photocatalysis. *Chemical Society Reviews*. 2014;**43**(16):5982-5993
- [59] Zhu S, Wang D. Photocatalysis: Basic principles, diverse forms of implementations and emerging scientific opportunities. *Advanced Energy Materials*. 2017;**7**(23):1700841
- [60] Sinai J, Sugarmen C, Fisher U. Adaptation and modification of gas turbines for solar energy applications. In: *Proceedings of GT2005 ASME Turbo Expo 2005; 6-9 June 2005; Power for Land Sea and Air: Reno-Tahoe, Nevada, USA*. 2005
- [61] Sinai J, Sugarmen C, Fisher U. GT2005-68122 balance of plant German aerospace agency. In: *Proceedings of GT2005 ASME Turbo Expo 2005; 6-9 June 2005; Power for Land, Sea and Air: Reno-Tahoe, Nevada, USA*. 2005
- [62] Atputharajah A. Operational challenges of low power hydro plants. In: *Handbook of Renewable Energy Technology*. Singapore: World Scientific Publishing Co. Pte. Ltd.; 2011;469-483

[63] Xia PJ, Chen FQ. Landscape pattern of the Xiangjiaba hydropower project'disturbed area in 2012 based on the GIS analysis. In: *Advanced Materials Research*. Trans Tech Publications. 2014;**955**:3854-3858

IntechOpen

IntechOpen

# We are IntechOpen, the world's leading publisher of Open Access books Built by scientists, for scientists

6,300

Open access books available

171,000

International authors and editors

190M

Downloads

Our authors are among the

154

Countries delivered to

TOP 1%

most cited scientists

12.2%

Contributors from top 500 universities



WEB OF SCIENCE™

Selection of our books indexed in the Book Citation Index  
in Web of Science™ Core Collection (BKCI)

Interested in publishing with us?  
Contact [book.department@intechopen.com](mailto:book.department@intechopen.com)

Numbers displayed above are based on latest data collected.  
For more information visit [www.intechopen.com](http://www.intechopen.com)



# Desalination with Renewable Energy: A 24 Hours Operation Solution

*Muhammad Wakil Shahzad, Muhammad Burhan,  
Doskhan Ybyraiymkul and Kim Choon Ng*

## Abstract

The inevitable escalation in economic development has serious implications on energy and environment nexus. The International Energy Outlook 2016 (IEO2016) predicted that the Non Organization for Economic Cooperation and Development (non-OECD) countries will lead with 71% rise in energy demand in contrast with only 18% in developed countries from 2012 to 2040. In Gulf Cooperation Council countries (GCC) countries, about 50% of primary energy is consumed for cogeneration based power and desalination plants. The desalination capacities are expected to increase fivefold by 2050 and renewable energy application can be one of the solution for sustainable water production. The major bottleneck in commercialization of renewable energy sources is its intermittent nature of supplies specially wind and solar. We proposed solar thermal energy storage to operate desalination system around the clock. Magnesium oxide (MgO) can be utilized as an efficient energy storage system to store solar thermal energy for off period operation. The heat generated by regeneration processes at day time and exothermic adsorption at night can operate desalination cycle 24 h. The operational temperature ranges from 120 to 140°C and energy storage 41–81 kJ/mol. It was successfully demonstrated by experimentation that MgO operated hybrid desalination cycle can achieve highest performance and lowest carbon emission. The proposed cycle can achieve sustainable water production goals.

**Keywords:** renewable energy, hybrid desalination, low emission desalination, sustainable desalination, energy storage

## 1. Introduction

The energy demand in Gulf Cooperation Council (GCC) countries is almost doubled in a decades, from 300 TWh in 2000 to 600 TWh in 2012. In GCC countries, the residential and commercial sector energy demand has grown rapidly. The residential sector consumes over 50% due to improved living standards. In GCC countries, per capita primary energy consumption is the highest as compared to other countries in the world as shown in the **Figure 1** [1–3].

The GCC countries also produce substantial amount of CO<sub>2</sub> and it was estimated as 1.2 billion tons of CO<sub>2</sub>-equivalent in 2012. The major part of CO<sub>2</sub> emission is related to energy and water production. The GCC countries are the most water

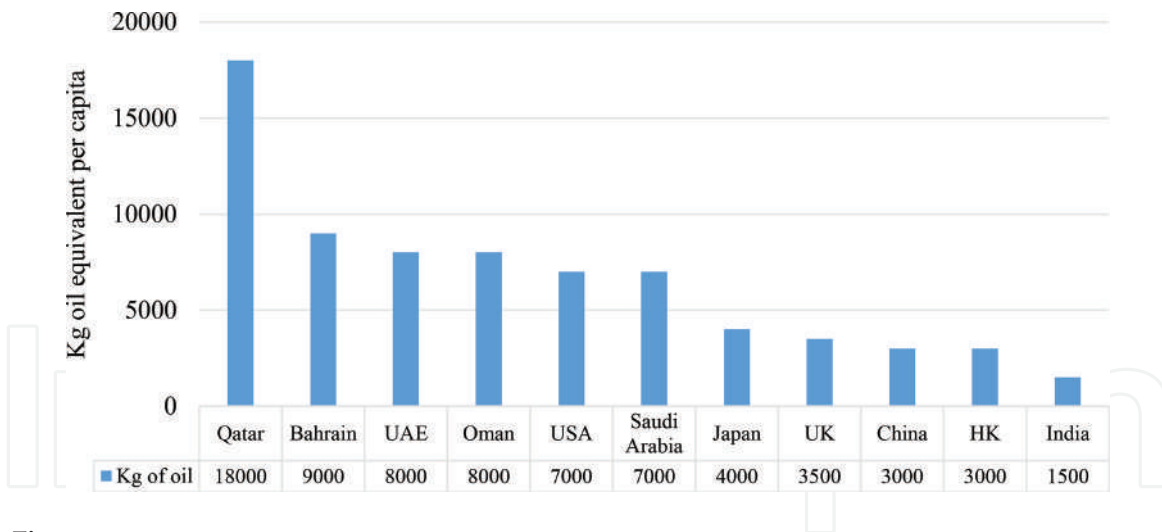


**Figure 1.**  
Per capita oil consumption in different parts of the world.

Country	2010 consumption	2050 consumption	2050 shortage
Bahrain	227	400	380
Kuwait	509	1220	850
Oman	760	1700	1150
Qatar	328	400	175
Saudi Arabia	20,480	27,000	20,100
UAE	3375	3500	3250
Total			

**Table 1.**  
Water consumption and estimated shortage in 2050 in GCC countries.

scariest in the world due to dry environmental conditions and recently it became even worst due to population increase and GDP growth. It is estimated that by 2050, the shortage of water supply can be as high as 77%. **Table 1** shows the water consumption and shortage in million cubic meter per year scenario in all GCC countries by 2050. It can be noticed the large gap in water demand and supply cannot be filled by renewable and ground water sources. The non-renewable such as desalination is the only source for future water supplies in GCC countries [1–3].

Today, all desalination processes are energy intensive and consume primary energy in the range of 6–10 kWh/m<sup>3</sup>. The inefficiency of desalination processes, 10–13% of thermodynamic limit, requires not only more energy but they also emit enormous CO<sub>2</sub> [4–7]. For future sustainability, one feasible option is to utilize renewable energy such as wind and solar. The renewable technologies have drastically developed and their economics are greatly improved in recent years, and GCC countries have great potential to exploit the renewable energies potential such as solar and wind. The GCC countries government announced mega investment plans to invest in renewable energy sectors to meet the increasing demand of electricity as shown in **Figure 2** [8].

The resettlement of energy mix in GCC countries needs a comprehensive plan for contractor as well as operator companies. One of the major challenges in renewable energies development is its intermittent nature. Currently they are only employed to cope the peak load typically during office hours. The one of the solution to overcome intermittent supply is the energy storage and there are two methods namely, battery storage and thermal heat storage. In terms of battery storage, the efficiency is very low, typically 8–10% in field operation due to

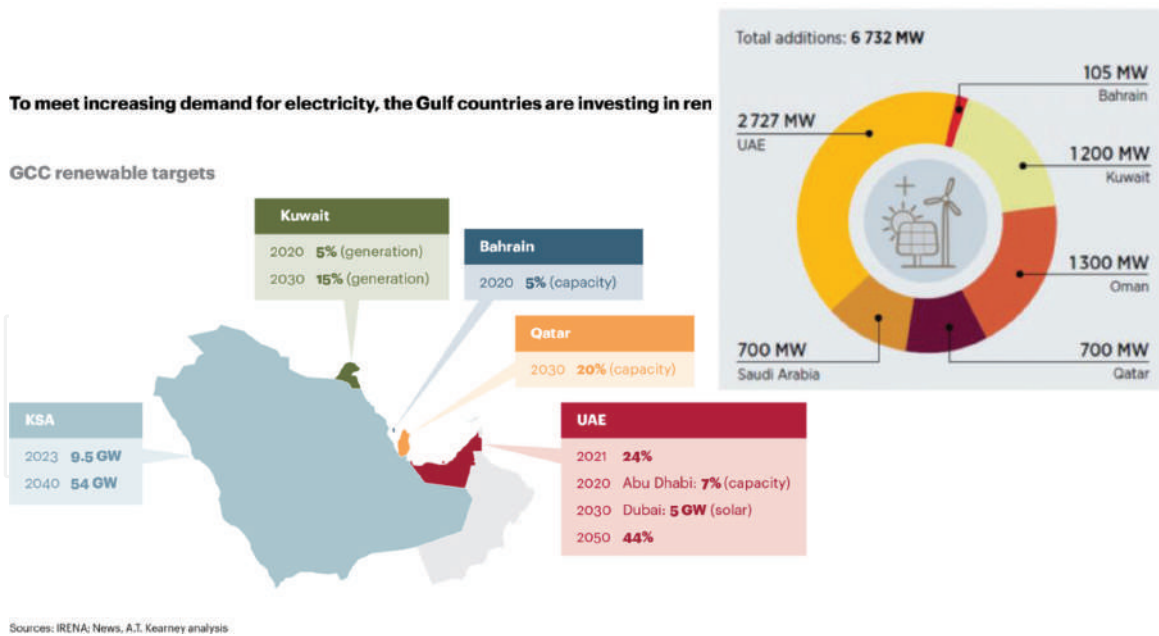


**Figure 2.**  
 GCC countries renewable energy development plan by 2030.

Materials	Heat storage method		Heat storage density (GJ/m <sup>3</sup> )	Heat charging temperature (°C)
Co <sub>3</sub> O <sub>4</sub>	Thermochemical materials (TCM)	Inorganic oxides	5.0	925
CaO			4.5	550
MgO			3.4	350
MgSO <sub>4</sub>		Anhydrate	2.6	125
Silica gel		Adsorbate	0.8	85
Zeolite			0.6	220
Paraffin	Phase change materials		0.2	60
Water	Sensible		0.2	0–100

**Table 2.**  
 Comparison of different thermal energy storage materials.

efficiencies involved from one form to other form conversions. On the other hand, direct thermal storage and utilization efficiency is significantly high due to same form of energy utilization without conversion into different forms. There are three major technologies utilize different methods to store solar energy. The comparison of different heat storage materials is summarized in **Table 2** [9–11].

## 2. Solar thermal energy storage and desalination application

Thermochemical materials (TCM) have many advantages over the other materials such as high heat storage density and low heat leak. Once the reactant leave the thermochemical materials, the enthalpy remains same and it help to achieve the state of energy charging. Subsequently, the discharged energy is utilized while the material remains stable. In the past, a lot of studies were carried out on heat pump using different TCM materials [12–14]. The selection of TCM materials for different application is based on many elements such as (i) heat storage temperature, (ii) heat releasing temperature,

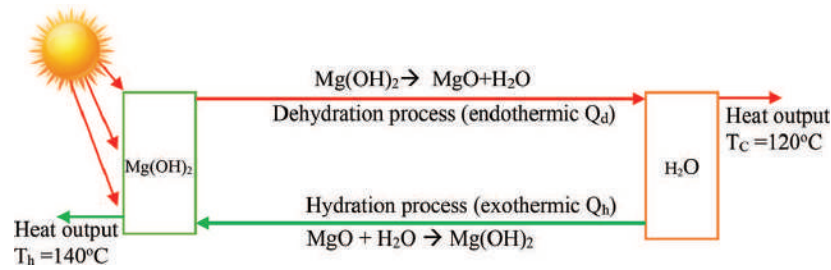


**Figure 3.**  
*MgO thermal energy storage system operation.*

(iii) heat storage density, and (iv) material stability. The magnesium oxide (MgO) is most suitable for thermal heat storage as compared to other materials due to its high density and stability. Many researchers published data on MgO thermal heat storage and its performance improvement [15, 16].

The dry MgO reacts with water (hydration) to become hydrated  $\text{Mg}(\text{OH})_2$ . The hydration is an exothermic reaction and generates 81 kJ/mol. During dehydration of  $\text{Mg}(\text{OH})_2$  it becomes MgO through a reverse process at 350–500°C from solar collectors and high temperature vapor are utilized as a heat source. It can be noticed that MgO as an energy storage material produce heat during day as well as night time. The hydration process at night and dehydration process at day with solar energy can produce sufficient heat energy to operate the desalination cycle.

The principle of this heat pump is shown in **Figure 3**. The heat pump consists of a magnesium oxide reactor and a water reservoir. In heat storage mode magnesium hydroxide ( $\text{Mg}(\text{OH})_2$ ) is dehydrated by surplus heat ( $Q_d$ ) at  $T_d$  from sun. The generated vapors are condensed at the reservoir at  $T_c$  and the condensation heat ( $Q_d$ ) of the vapor is used for desalination cycle at day time. The hydration of magnesium oxide proceeds in the reactor by introducing the vapor, and a hydration heat output ( $Q_h$ ) at  $T_h$  is generated to operate desalination cycle at night. Thermal drivability, which does not require mechanical work, is one of the advantages of the heat pump. The environmentally friendly and economical nature of the reactants is also advantageous. This type of heat pump is able to store heat at around 350°C through  $\text{Mg}(\text{OH})_2$  dehydration and to transfer stored heat at temperatures between 110 and 150°C through MgO hydration. The solar thermal energy storage and 24 h delivery around 100°C is best suitable for sustainable desalination processes [17–19].

The renewable energy (RE) driven desalination processes are already commercialized but at low scale due to some operational complexity. **Table 3** summarized

Plant name	Location	Technology	Capacity	Energy source	Cost* (US\$/m <sup>3</sup> )
Kimolos	Greece	MED	2000	Geothermal	2.5–3
Keio university	Japan	MED	100	Solar thermal	
PSA	Spain	MED	72	CSP	
Ydriada	Greece	RO	80	Wind	2–6
Morocco	Morocco	RO	20	PV	2–5
Oyster	Scotland	RO	—	Wave energy	3–5
KAUST**	Saudi Arabia	MEDAD hybrid	10	Solar thermal	0.5

\*Cost is estimated based on plant capacity more than 1000 m<sup>3</sup>/day [20].

\*\*Refs. [21–29].

**Table 3.**  
*RE driven desalination technologies and water cost.*

the major renewable desalination plants operated in the world and estimated cost of water production.

It can be noticed that thermal desalination processes are most favorable option with solar thermal energy operation. The most efficient thermally driven multi effect desalination (MED) system recently investigated to overcome its conventional operational limitations. The numbers of stages in a MED is controlled by top brine temperature (TBT) and lower brine temperature (LBT). The TBT typically  $70^{\circ}\text{C}$  is restricted by soft scaling components in the feed water and the LBT is controlled by ambient condition due to water cooled condenser to condense the last stage vapors. The MED system can be more efficient if these two limitations can be removed to increase number of recoveries. Researchers found that TBT can be increased to  $125^{\circ}\text{C}$  by inducing nano-filtration (NF) prior to introduction the feed into the system. This NF process helps to remove soft scaling components and prevent scaling and fouling on the tubes of evaporators. The inter stage temperature and the last stage operating temperature limitations can be overcome by hybridization with adsorption cycle. AD cycle can operate below ambient conditions typically as low as  $5^{\circ}\text{C}$  due high affinity of water vapors of adsorbent (silica gel). MED last stage temperature can be lower down to  $5^{\circ}\text{C}$  by introducing the AD at downstream. The proposed hybrid MEDAD system with TES will be the best choice for sustainable water supplies.

### 3. Proposed system operation

The detailed schematic of TES driven hybrid MEDAD desalination cycle is shown in **Figure 4**. During day time operation, solar heat is supplied to the hydrated  $\text{Mg}(\text{OH})_2$  at  $300\text{--}400^{\circ}\text{C}$  and regenerated vapor condensation heat at  $120\text{--}150^{\circ}\text{C}$  is utilized to operate desalination cycle. At night time, the hydration of  $\text{MgO}$  generates sufficient heat due to exothermic reaction that is supplied to the desalination cycle to continue the operation. It can be noticed that with  $\text{MgO}$  energy storage system, thermal desalination can be operated for 24 h using solar energy.

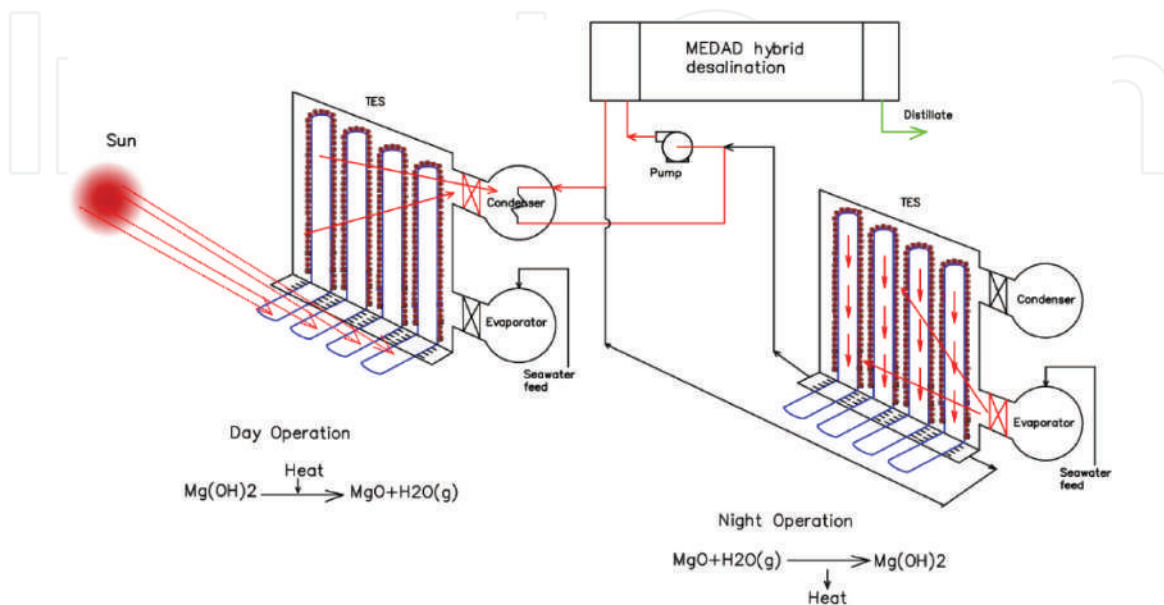


**Figure 4.**  
Proposed TES driven hybrid MEDAD desalination cycle.

## 4. Experimentation

An experimental system was designed and installed to test workability of proposed concept. **Figure 5** shows the temperature profiles of MEDAD effects at heat source of 45°C. The pilot was tested at different temperatures to investigate the performance. **Figure 6** shows the hybrid MEDAD system effects temperatures at different heat source temperatures. The system performed well as per designed 3–4°C inter-effect temperature difference. Similarly, **Figure 7** shows the corresponding saturation pressures.

**Figure 8** shows the water production profiles of MED effects, AD condenser and total production at 45°C heat source temperature. The summary of water production presented in **Figure 9** at different heat source temperatures. It can be seen that at higher temperature the water production is also higher and it drop due to drop in heat capacity. The system is designed for 45°C operational temperature but it performed well at off-design conditions. It shows the robustness of the thermally driven desalination systems.

The thermal energy consumed is shown in **Figure 10**. It can be noticed that at higher heat input temperature the energy consumed by the system is also higher. It is mainly due to the higher temperature difference between heat inlet and out

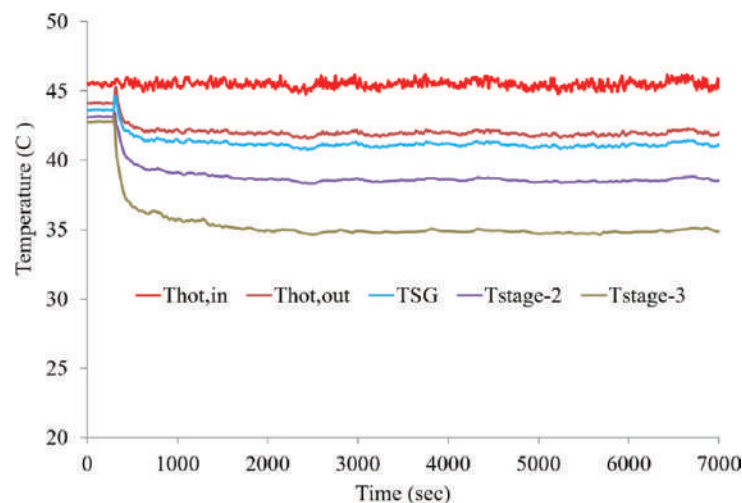


**Figure 5.**  
Hybrid MEDAD temperature profiles at 45°C heat source.

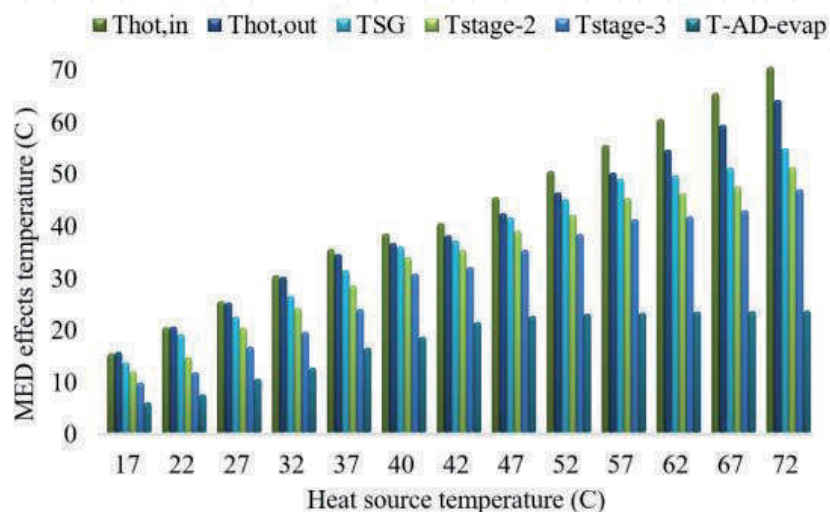


**Figure 6.**  
Hybrid MEDAD inter-effect temperatures at different heat source (reproduce with author's permission [30]).

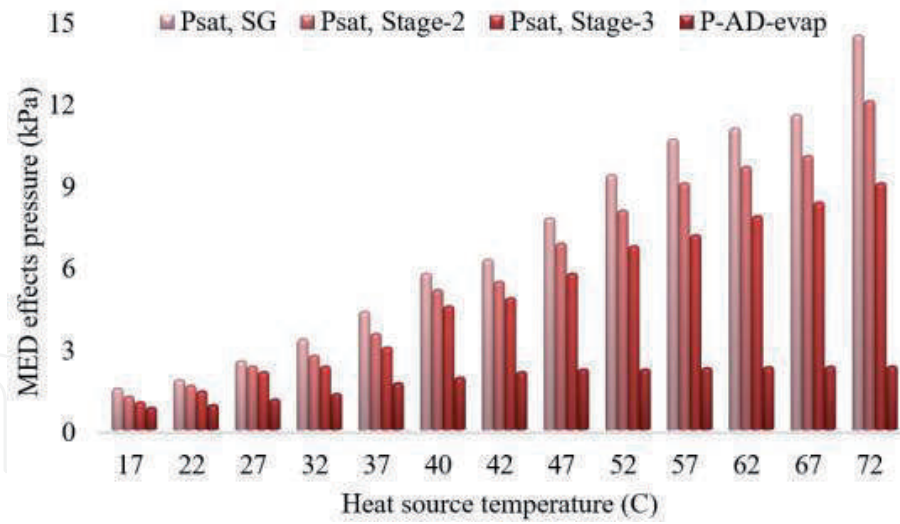


**Figure 7.** Hybrid MEDAD inter-effect pressures at different heat source (reproduce with author's permission [30]).

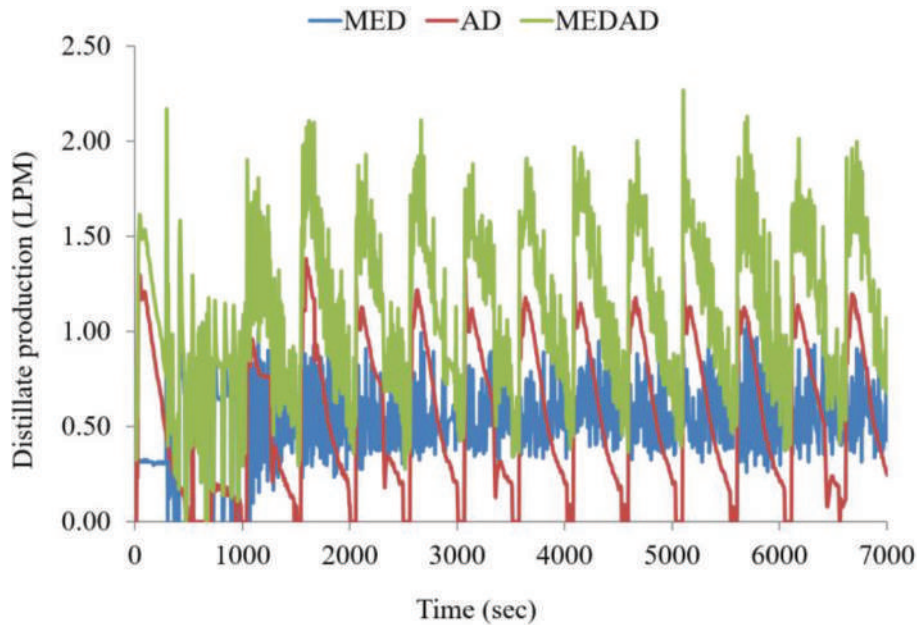


**Figure 8.** Hybrid MEDAD water production profiles at 45°C heat source (reproduce with author's permission [30]).

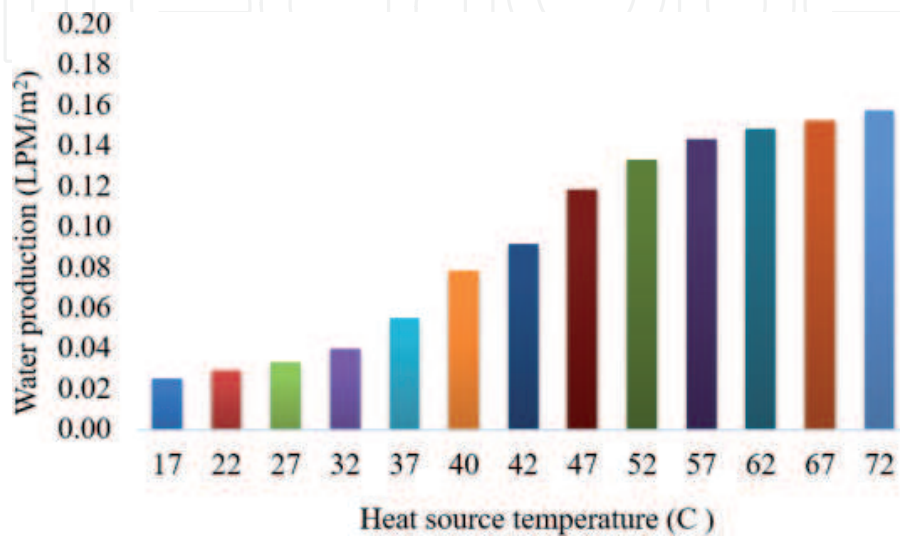


**Figure 9.** Hybrid MEDAD water production at different heat source temperature (reproduce with author's permission [30]).

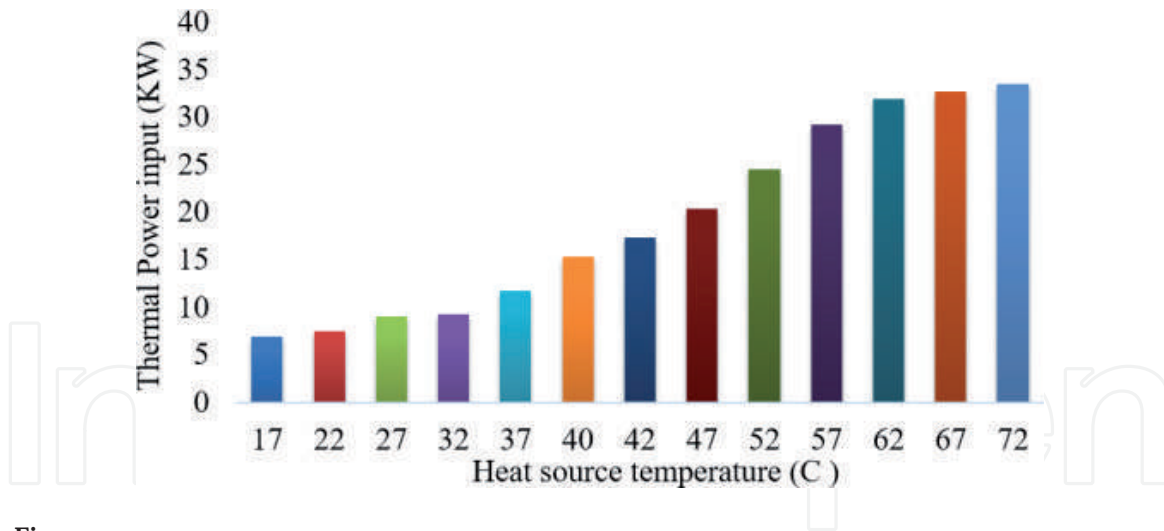


**Figure 10.** Hybrid MEDAD thermal energy input at different heat source temperature (reproduce with author's permission [30]).

temperatures. The interesting trend was noticed at below 25°C where heat input showed negative value. It is because the heat was scavenged from the ambient. The system was operating below ambient conditions due to adsorption cycle hybridization that allows last effects to operate as low as 5°C.

The successful experimentation of hybrid MEDAD cycle proved the workability of TES + MEDAD system for future sustainable water supplies.

## 5. Conclusion

Thermal energy storage based hybrid desalination system is proposed for 24 h operation. MgO has high energy density and stability for long term operation. The proposed TES + MEDAD hybrid cycle has highest performance. The superiority of MEDAD cycle has been successfully demonstrated pilot as compared to conventional MED system by improving water production to twofold as same heat source temperature. The proposed combination is estimated to have highest performance to achieve sustainability goals. These innovative solutions will help to save energy and protect environment.

## Acknowledgements

Authors would like to thanks to KAUT and NUS for this study. The data is reproduced by PI and the author's permission [30].

## Nomenclature

OECD	Organization for Economic Cooperation and Development
GCC	Gulf Cooperation Council
GDP	gross domestic product
UAE	United Arab Emirates
TCM	thermochemical materials
RE	renewable energy
MED	multi effect desalination

MSF	multi stage flash
SWRO	seawater reverse osmosis
AD	adsorption
TES	thermal energy storage
CSP	concentrated solar photovoltaic
TBT	top brine temperature
LBT	lower brine temperature
LPM	liter per minute

IntechOpen

### **Author details**

Muhammad Wakil Shahzad\*, Muhammad Burhan, Doskhan Ybyraiymkul and Kim Choon Ng

Water Desalination and Reuse Centre (WDRC), Biological and Environmental Science and Engineering (BESE), King Abdullah University of Science and Technology, Saudi Arabia

\*Address all correspondence to: [muhammad.shahzad@kaust.edu.sa](mailto:muhammad.shahzad@kaust.edu.sa)

### **IntechOpen**

© 2019 The Author(s). Licensee IntechOpen. This chapter is distributed under the terms of the Creative Commons Attribution License (<http://creativecommons.org/licenses/by/3.0>), which permits unrestricted use, distribution, and reproduction in any medium, provided the original work is properly cited. 

## References

- [1] Energy Use (kg of Oil Equivalent Per Capita). World Bank Data. Available from: <https://data.worldbank.org/indicator/EG.USE.PCAP.KG.OE> [Accessed: Jan 02 2019]
- [2] Renewable Energy Market Analysis. The GCC region. The International Renewable Energy Agency (IRENA) Report 2016
- [3] Parmigiani L. Water and Energy in the GCC: Securing Scarce Water in Oil-Rich Countries. The Institut français des relations internationales (Ifri) Report 2015. ISBN: 978-2-36567-442-3
- [4] Shahzad MW, Burhan M, Ng KC. A standard primary energy approach for comparing desalination processes. *Nature Clean Water*. 2019;**1**:1-7
- [5] Shahzad MW, Burhan M, Ybyrainkul D, Ng KC. Desalination processes efficiency and future roadmap. *Entropy*. 2019;**21**(1):84
- [6] Shahzad MW, Burhan M, Son HS, Seung Jin O, Ng KC. Desalination processes evaluation at common platform: A universal performance ratio (UPR) method. *Applied Thermal Engineering*. 2018;**134**:62-67
- [7] Ng KC, Shahzad MW, Son HS, Hamed OA. An exergy approach to efficiency evaluation of desalination. *Applied Physics Letters*. 2017;**110**:184101. DOI: 10.1063/1.4982628
- [8] Partner, Kearney AT. Why oil-rich gulf countries need to invest in renewable energy. World Economic Forum. Available from: <https://www.weforum.org/agenda/2017/05/why-oil-rich-gulf-countries-need-to-invest-in-renewable-energy/> [Accessed: Jan 15 2019]
- [9] Yim T, Kim HS, Lee JY. Cyclic assessment of magnesium oxide with additives as a thermochemical material to improve the mechanical strength and chemical reaction. *Energies*. 2018;**11**:2366
- [10] Singh A, Tescari S, Lantin G, Agrafiotis C, Roeb M, Sattler C. Solar thermochemical heat storage via the  $\text{Co}_3\text{O}/\text{CoO}$  looping cycle: Storage reactor modelling and experimental validation. *Solar Energy*. 2017;**144**:453-465
- [11] Fernandes MS, Brites GJV, Costa JJ, Gaspar AR, Costa VAF. Modeling and parametric analysis of an adsorber unit for thermal energy storage. *Energy*. 2016;**102**:83-94
- [12] Cabeza LF, Martorell I, Miró L, Fernández AI, Barreneche C. *Advances in Thermal Energy Storage Systems: Methods and Applications, Advances in Thermal Energy Storage Systems*. Woodhead Publishing. ISBN: 978-1-78242-088-0
- [13] Alva G, Lin Y, Fang G. An overview of thermal energy storage systems. *Energy*. 2018;**144**:341-378
- [14] Thomas JJ, Musso S, Prestini I. Kinetics and activation energy of magnesium oxide hydration. *The American Ceramic Society Journal*. 2014;**97**:275-282
- [15] Mastronardo E, Kato Y, Bonaccorsi L, Piperopoulos E, Milone C. Thermochemical storage of middle temperature wasted heat by functionalized C/Mg(OH) hybrid materials. *Energies*. 2017;**10**:70
- [16] Mastronardo E, Kato Y, Bonaccorsi L. *Piperopoulos elpida*, efficiency improvement of heat storage materials for  $\text{MgO}/\text{H}_2\text{O}/\text{Mg}(\text{OH})_2$  chemical heat pumps. *Applied Energy*. 2016;**162**:31-39
- [17] Kato Y, Takahashi F, Sekiguchi T, Ryu J. Study on medium temperature chemical

heat storage using mixed hydroxides. *International Journal of Refrigeration*. 2009;**32**:661-666

[18] Kato Y, Nakahata J, Yoshizawa Y. Durability characteristics of the hydration magnesium oxide under repetitive reaction. *Journal of Material Sciences*. 1999;**34**:475-480

[19] Kato Y, Yamashita N, Kobayashi K, Yoshizawa Y. Kinetic study of the hydration of magnesium oxide for a chemical heat pump. *Applied Thermal Engineering*. 1996;**16**:853-862

[20] Alkaisi A, Mossad R, Sharifian-Barforoush A. A review of the water desalination systems integrated with renewable energy. *Energy Procedia*. 2017;**110**:268-274

[21] Shahzad MW, Burhan M, Ang L, Ng KC. Energy-water-environment nexus underpinning future desalination sustainability. *Desalination*. 2017;**413**:52-64

[22] Shahzad MW, Ng KC. An improved multi-evaporator adsorption desalination cycle for GCC countries. *Energy Technology*. 2017. DOI: 10.1002/ente.201700061

[23] Shahzad MW, Ng KC, Thu K. Future sustainable desalination using waste heat: Kudos to thermodynamic synergy. *Environmental Science: Water Research & Technology*. 2016;**2**:206-212

[24] Thu K, Kim Y-D, Shahzad MW, Saththasivam J, Ng KC. Performance investigation of an advanced multi-effect adsorption desalination (MEAD) cycle. *Applied Energy*. 2015;**159**:469-477

[25] Shahzad MW, Thu K, Kim Y-d, Ng KC. An experimental investigation on MEDAD hybrid desalination cycle. *Applied Energy*. 2015;**148**:273-281

[26] Ng KC, Thu K, Oh SJ, Ang L, Shahzad MW, Ismail AB. Recent

developments in thermally-driven seawater desalination: Energy efficiency improvement by hybridization of the MED and AD cycles. *Desalination*. 2015;**356**:255-270

[27] Shahzad MW, Ng KC, Thu K, Saha BB, Chun WG. Multi effect desalination and adsorption desalination (MEDAD): A hybrid desalination method. *Applied Thermal Engineering*. 2014;**72**:289-297

[28] Ng KC, Thu K, Shahzad MW, Gee CW. Progress of adsorption cycle and its hybrids with conventional multi-effect desalination processes. *IDA Journal of Desalination and Water Reuse*. 2016;**6**:1, 44-56

[29] Shahzad MW, Thu K, Saha BB, Ng KC. An emerging hybrid multi-effect adsorption desalination system. *Evergreen Joint Journal of Novel Carbon Resource Sciences & Green Asia Strategy*. 2014;**01**:02, 30-36

[30] Muhammad Wakil Shahzad, The hybrid multi-effect desalination (MED) and the adsorption (AD) cycle for desalination, Doctoral Thesis, National University of Singapore. 2013

# We are IntechOpen, the world's leading publisher of Open Access books Built by scientists, for scientists

6,300

Open access books available

171,000

International authors and editors

190M

Downloads

Our authors are among the

154

Countries delivered to

TOP 1%

most cited scientists

12.2%

Contributors from top 500 universities



WEB OF SCIENCE™

Selection of our books indexed in the Book Citation Index  
in Web of Science™ Core Collection (BKCI)

Interested in publishing with us?  
Contact [book.department@intechopen.com](mailto:book.department@intechopen.com)

Numbers displayed above are based on latest data collected.  
For more information visit [www.intechopen.com](http://www.intechopen.com)



## Chapter

# Nonconventional Wastewater Treatment for the Degradation of Fuel Oxygenated (MTBE, ETBE, and TAME)

*Zenaida Guerra Que, José Gilberto Torres Torres, Ignacio Cuauhtémoc López, Juan C. Arévalo Pérez, Adrian Cervantes Uribe, Hermicenda Pérez Vidal, Alejandra E. Espinosa de los Monteros Reyna, José G. Pacheco Sosa, María A. Lunagómez Rocha and Cecilia Sánchez Trinidad*

## Abstract

Catalytic wet air oxidation (CWAO) is a nonconventional wastewater treatment, consisting of oxygen pressure releasing inside a reactor in order to degrade organic compounds dissolved in water, using a solid catalyst in the presence of an activated  $O_2$  species, usually at temperatures ranges of 125–250°C and pressures of 10–50 bar. CWAO can reduce operating costs of conventional treatment due to the use of ideal catalyst that is able to improve reaction conditions at temperatures and pressures as mild as possible, simultaneously setting high catalytic activity and long-term stability of heterogeneous catalysts. Oxygenated fuels are gasoline additives in reformulated gasoline and oxyfuels. In the beginning, they provided an alternative solution of environmental problems, such as greenhouse gas emissions and octane enhancement, caused by fossil fuel use. The oxygenated fuels frequently used are methyl tert-butyl ether (MTBE), ethyl tert-butyl ether (ETBE), and tert-amyl methyl ether (TAME). However, there is environmental impact from oxygenated fuel hydrocarbons related to widespread contamination of groundwater and other natural waters. Our research group developed a wide study in order to evaluate several catalysts (Ru, Au, Cu, and Ag supported on  $Al_2O_3$ ,  $Al_2O_3$ - $CeO_2$ , and  $TiO_2$ - $CeO_2$ ) and to obtain the best for the efficiency of the oxidation process.

**Keywords:** nanoparticles, wastewater, CWAO, fuel oxygenated

## 1. Introduction

### 1.1 Oxygenated fuels

Oxygenated fuels are oxygen-rich compounds such as alcoholic and ether fuels that act as gasoline additives in reformulated gasoline and oxyfuels. Oxygenates can be

blended into gasoline in two forms: alcohols (such as methanol or ethanol) or ethers. They have potential to provide an alternative solution of environmental problems caused by fossil fuel use. The oxygenated ether fuels used more frequently are methyl tert-butyl ether (MTBE), ethyl tert-butyl ether (ETBE), and tert-amyl methyl ether (TAME), although the first fuel oxygenate used in reformulation was MTBE. The use of MTBE as an octane enhancer in the United States began in 1979 [1, 2].

MTBE is a compound (chemical formula  $C_5H_{12}O$ ) that is synthesized by the chemical reaction of methanol and isobutylene, and it is almost exclusively used as a fuel additive in motor gasoline. Although ETBE and TAME have only secondary importance in production industry, recently they have become more prevalent, and they can be used instead of MTBE. In France, MTBE has been partially replaced by the ETBE since 1990 or as part of a “binary or ternary mixture” with MTBE [3–5].

ETBE (chemical formula  $C_6H_{14}O$ ) is considered an attractive octane enhancer as it presents a lower Reid vapor pressure (RVP) mixture and lower water solubility than MTBE and ethanol. The azeotropic mixture of ETBE with ethanol takes down the volatility of ethanol making it suitable as an additive for automatic gasoline [6, 7].

Finally, TAME (chemical formula  $C_6H_{14}O$ ) was considered as an oxygenated fuel until the 1990s despite its octane rating lower than other oxygenated fuels; besides it is very soluble with other ethers, and it is highly soluble in water (12 g/l) [8, 9].

## 1.2 Importance of oxygenated fuels in petroleum industry

The leading produced fuel in the world is gasoline. Because of its widespread use and the fact that it is composed of that fraction of crude oil with lower boiling points, gasoline is the single largest source of volatile hydrocarbons to the environment. Motor gasoline comes in various blends with properties that affect engine performance. All motor gasolines are made of relatively volatile components of crude oil. Other fuels include distillate fuel oil (diesel fuel and heating oil), jet fuel, residual fuel oil, kerosene, aviation gasoline, and petroleum coke. In the petroleum refining process, heat distillation is used first to separate different hydrocarbon components. The lighter products are liquefied petroleum gases and gasoline, whereas the heavier products include heavy gas oils. Liquefied petroleum gases include ethane, ethylene, propane, propylene, n-butane, butylenes, and isobutane. Internal combustion engines of high compression ratio require gasoline with octane ratings that are sufficiently high to ensure efficient combustion [2, 10, 11].

Gasolines need additives that increase their octane rating so they can decrease their self-knock capacity, increasing their resistance to compression, and finally improve the quality of gasoline. An economical way of achieving these properties has been the use of anti-knock additives, such as tetraethyl and tetramethyl lead at concentrations up to 0.84 g/l. With the phasing out of lead from gasoline because it was increasingly recognized that lead is toxic and non-biodegradable, oxygenated fuel became a better alternative for gasoline additive, instead of lead. Oxygenated fuels act as octane enhancers, bringing the additional benefit of making gasoline burn almost completely. Actually, using oxygenated fuels in internal combustion engine leads to a reduction of greenhouse gas (GHG) emissions, compared to gasoline because they burn cleaner than regular gasoline and produce lesser carbon monoxide (CO) and nitrogen oxides (NO<sub>x</sub>) and they reduce emissions of unburned hydrocarbons. Furthermore, using oxygenated fuels in an internal combustion engine (ICE) provides an alternative to conventional fuels that can solve many environmental problems [6, 12, 13].

In the United States, air quality regulations placed on automobile exhaust gases have forced dramatic changes in gasoline formulations. By 1990, the Clean Air Act Amendments (CAAA) required additives, such as MTBE at 15% and ethanol, to be

blended in gasoline in some metropolitan areas, heavily polluted by carbon monoxide, and to reduce carbon monoxide and ozone concentrations [14].

### 1.3 Environmental impact of oxygenated fuels

Despite providing better conditions in terms of fuel quality, an environmental impact from oxygenated fuel hydrocarbons related to widespread contamination of groundwater and other natural waters exists. The distribution and storage of crude oil and refined products result in releases of significant amounts of hydrocarbons to the atmosphere, surface waters, soils, and groundwater. Groundwater contamination by crude oil, and other petroleum-based liquids, is a particularly widespread problem. In Mexico, the agency in charge of producing and distributing fuels derived from petroleum distillation, such as gasoline, diesel, fuel oil, diesel, and LP gas, is *Petróleos Mexicanos (PEMEX)*. The retail distribution of gasoline and diesel is carried out by service stations (gas stations). One of the environmental risks that involves the handling of these stations is spills or leaks of fuels, which cause the contamination of the sites where the storage tanks are located [15].

Unfortunately, these oxygenates have high water solubility and high volatility, causing a high concentration of oxygenated fuel in the environment, air, and water. Another important problem happens when oxygenated fuel is accumulated in the groundwater due to it not absorbing appreciably to soil and undergoing only in slow biodegradation compared to the benzene, toluene, ethylbenzene, and the xylenes (BTEX) in gasoline. The relatively recalcitrant nature of oxygenated fuel to microbial attack makes them persistent, due to them being refractory to the biological treatments. Because of the chemical structure of these, oxygenated fuel hinders their natural biodegradation, which contains a combination of two biorecalcitrant organic functional groups: the ether bond and tertiary carbon atom. These are the reasons why water supplies close to the production sites of MTBE, ETBE, and TAME or near underground petroleum storage tanks and fuelling stations are often contaminated by large amounts of these compounds [16, 17].

There have been extensive occurrences of groundwater contamination by MTBE in the United States because of its prevailing use. In a sampling study of 1208 domestic wells in the United States, MTBE was the most frequently detected fuel oxygenate and the eighth most commonly detected VOC. Perhaps the most publicized case of MTBE contamination of groundwater is the one involving public water supply wells in Santa Monica, California. In August 1995, the city of Santa Monica discovered MTBE in wells used for drinking water supply through routine analytical testing of well water [18, 19].

MTBE has been detected in snow, storm water, surface water (streams, rivers, and reservoirs), groundwater, and drinking water, based on limited surveillance operations conducted in the United States. MTBE concentrations found in storm water ranged from 0.02 to 8.7  $\mu\text{g/l}$ , with a median value of less than 1.0  $\mu\text{g/l}$ . In streams, rivers, and reservoirs, the detection range was 0.2–30  $\mu\text{g/l}$ , and the range of median values in several studies was from 0.24 to 7.75  $\mu\text{g/l}$  [5, 19].

In fact, the US Environmental Protection Agency (USEPA) included MTBE in its Contaminant Candidate List. MTBE in drinking water is carcinogenic for humans and animals. USEPA established a drinking water health advisory of 20–40  $\mu\text{g/l}$  MTBE in December 1997, because it is hazardous to human health (US Environmental Protection Agency, 1997).

Although alternative ether oxygenates are detected less frequently than MTBE, these alternative oxygenates show future groundwater contaminations similar to MTBE if they are not under control.

The toxicokinetic data on MTBE in people come mainly from controlled studies of healthy adult volunteers and in a population exposed to oxygenated gasoline. MTBE quickly passes into circulation after inhalation exposure. In healthy volunteers exposed to inhalation, MTBE kinetics was linear up to concentrations of  $268 \text{ mg/m}^3$  (75 ppm). It was measured in the blood and urine of people exposed to tertiary butyl alcohol, metabolic MTBE. The maximum blood concentrations of tertiary butyl alcohol were  $17.2\text{--}1144 \text{ }\mu\text{g/m}^3$  and  $7.8\text{--}925 \text{ }\mu\text{g/m}^3$ , respectively, in people exposed between  $5.0$  and  $178.5 \text{ mg/m}^3$  (1.4–50 ppm) of MTBE. Based on a single-behavior model, rapid (36–90 min) and slow (19 h) components of MTBE half-life were identified (41). Following the introduction of two separate fuel programs in the United States, which require the use of gasoline oxygenation products, consumers in some areas have complained of acute health disorders, such as headaches, irritation of the eyes and nose, cough, nausea, dizziness, and disorientation. The acute experimental toxicity ( $CL_{50}$ ) of MTBE in fish, amphibians, and crustaceans is greater than  $100 \text{ mg/l}$ .

WAO consists of an oxidation in aqueous medium at high temperatures using pure oxygen or high pressure air as an oxidant to maintain the liquid phase. The pressures used and reported in the literature range from 20 to 200 bar and temperature between  $150$  and  $350^\circ\text{C}$ , making this process highly expensive for industrial application. The use of catalysts allows reducing the temperature and pressure conditions for oxidation and even increasing the selectivity toward  $\text{CO}_2$ . That is why we employ catalytic wet air oxidation, instead of WAO. CWAO of MTBE and oxygenated fuels of gasoline as ETBE and TAME is a nonconventional treatment for degradation of organic compounds in aqueous medium. Our research group developed a wide study in order to evaluate several catalysts and to know what the best are for the efficiency of oxidation process and the total mineralization of pollutants into  $\text{CO}_2$  and  $\text{H}_2\text{O}$ .

## **2. Synthesis, characterization, and catalytic activity of noble (Ru, Au, Ag) and based (Cu) metal nanoparticles supported applied in the CWAO of fuel oxygenated**

### **2.1 Synthesis of $\text{Al}_2\text{O}_3$ and $\text{Al}_2\text{O}_3\text{-CeO}_2$ by wet impregnation and precursor calcination**

The synthesis methods occupied for the production of supported catalysts include different techniques or procedures based on a phenomenon of precipitation, chemical adsorption, hydrolysis-polymerization, etc. These methods can synthesize supported catalysts in a single step, or in two steps, that is, both the precursor salt of the support and the active phase are added in the reaction mixture in a single step; otherwise, in sequential or two steps, first the support is synthesized, usually an oxide, and then the active phase, usually a metal, is prepared by some other specific method, expecting all the metal to be added and adsorbed on the support, without metal loss and with a high metal dispersion [20, 21].

These methods determine important properties such as homogeneous metal dispersion, high specific surface area, adequate acidity/basicity ratio, metal-support interaction, and generation of structural defects, for example, oxygen vacancies and reducibility; an improvement in the catalytic performance is concluded owing to the development of these properties in the synthesized catalysts [22, 23]. So in this, study we evaluated different synthesis methods for the catalysts tested in CWAO from oxygenated fuels.

The  $\gamma$ -alumina was obtained by the calcination of boehmite Catapal-B ( $\text{AlO}(\text{OH})$ ), in this process an amount of boehmite ( $\text{AlO}(\text{OH})$ ) is deposited in a

fixed-bed quartz reactor in which a continuous flow of air of 1 cm<sup>3</sup>/s is passed, and then the calcination is carried out, at a temperature of 650°C for 4 h.

Wet impregnation method was used to prepare the Al<sub>2</sub>O<sub>3</sub>-CeO<sub>2</sub> support. Ceria is incorporated into the boehmite (AlO(OH)) with an aqueous solution of Ce(NO<sub>3</sub>)<sub>3</sub>·6H<sub>2</sub>O (necessary amount of salt to obtain 1, 3, 5, 7.5, and 10% weight) in 100 ml of distilled water. The precursor solution of ceria is previously deposited in a ball flask, the boehmite is added to this solution and left to stir for 3 h in a rotary evaporator, and then the solution is dried with constant agitation at 60°C to evaporate the water excess. After impregnation, the obtained solid sample was dried at 120°C for about 16 h and calcined at a temperature of 650°C in air flow of 1 cm<sup>3</sup>/s for 4 h. The CeO<sub>2</sub> support was obtained commercially.

## 2.2 Synthesis of noble and base metal catalysts by wet impregnation

The solid catalysts reported in the literature that are used in the oxidation of water pollutants can be classified into four groups: supported metal oxides, unsupported metal oxides, supported metals, and mixtures of noble metals and metal oxides. The type of supported metal is composed mainly of noble and base metals. These are also very important to influence catalyst activity. Noble metals such as Ag, Au, Ru, Pd, Rh, and Pt are very active elements for oxidation reactions; they reveal high activities and excellent stability; however, their high cost and limited availability can decrease their applicability. Base catalysts such as Ni and Cu are more interesting systems, and a lot of research is being done to improve their stability because by having a lower cost, compared to noble metals, they are an economical option; they are also active, but less stable, and suffer from carbon deposit and metal leaching [24, 25].

Cu catalysts supported on Al<sub>2</sub>O<sub>3</sub> were synthesized by wet impregnation in a single step. A calculated amount of copper nitrate to obtain a concentration by weight of 5, 10 and 15wt% in copper plus an adequate amount of boehmite Catapal-B were dissolved in 100 ml of water; then the solution was adjusted to a pH of 1, with the addition of a drop of HNO<sub>3</sub>, and stirred for 4 h, regulating the temperature from 70 to 90°C. After impregnation, the obtained solid sample was dried at 120°C for about 12 h and calcined at a temperature of 400°C in airflow of 1 cm<sup>3</sup>/s for 4 h. Cu (5wt%)/Al<sub>2</sub>O<sub>3</sub>, Cu (10wt%)/Al<sub>2</sub>O<sub>3</sub>, and Cu (15wt%)/Al<sub>2</sub>O<sub>3</sub> are the monometallic Cu catalysts supported in alumina, synthesized by wet impregnation method in a single step, which later we will name as Cu<sub>5</sub>AlIH, Cu<sub>10</sub>AlIH, and Cu<sub>15</sub>AlIH.

Copper catalysts supported on Al<sub>2</sub>O<sub>3</sub> were also synthesized by sol-gel in a single step. An aqueous solution of 10 ml of aluminum trisecbutoxide ([C<sub>2</sub>H<sub>5</sub>CH(CH<sub>3</sub>)O]<sub>3</sub>Al), 97% aldrich, d = 0.96 g/mol with 4 g of urea and copper nitrate adequate amount in grams for the percentages of 5, 10, and 15wt% in 1-butanol was progressively added, between 70 and 90°C to a mixture of water and butanol, under constant stirring. After 24 h reflux at 70°C, the resulting pseudo-gel was dried in a rotating evaporator at 120°C for 12 h and then calcined at 400°C for 4 h. It is worth mentioning that a catalyst was prepared with a pyrrolidine additive instead of urea, exclusively with the same quantities of reagents as the 15wt% in Cu. The synthesized monometallic catalysts will be named as Cu<sub>5</sub>AlSG, Cu<sub>10</sub>AlSG, Cu<sub>15</sub>AlSG, and Cu<sub>15</sub>AlSGp.

Finally, the monometallic Cu/Al<sub>2</sub>O<sub>3</sub> catalysts were synthesized by wet impregnation with urea and with a concentration by weight of 5, 10, and 15wt% of the metal. A calculated amount of boehmite Catapal-B was dissolved in 300 ml of deionized water; then the solution was adjusted to a pH of 3 with the addition of 1 ml of HNO<sub>3</sub> and stirred for 2 h. After that, 200 ml of a solution of cupric nitrate [Cu(NO<sub>3</sub>)<sub>2</sub>·½H<sub>2</sub>O] and urea is added dropwise to the solution of boehmite Catapal-B, regulating the temperature from 70 to 90°C. After impregnation, the obtained solid

sample was washed three times with hot water and dried at 120°C, and finally it was calcined at a temperature of 400°C for 4 h. It should be noted that a catalyst was prepared with a pyrrolidine additive instead of urea, exclusively with the same amounts of reagents as the 15wt% in Cu. The synthesized monometallic catalysts will be named as Cu<sub>5</sub>AlIHU, Cu<sub>10</sub>AlIHU, Cu<sub>15</sub>AlIHU, and Cu<sub>15</sub>AlIHp.

Ru-supported catalysts were prepared by wet impregnation method of Al<sub>2</sub>O<sub>3</sub> and Al<sub>2</sub>O<sub>3</sub>-CeO<sub>2</sub> supports aggregating the appropriated amounts of an aqueous solution containing RuCl<sub>3</sub>\*XH<sub>2</sub>O to obtain a nominal concentration of 2wt% of Ru, adding 100 ml of hydrochloric acid 0.1 M. First Al<sub>2</sub>O<sub>3</sub> and Al<sub>2</sub>O<sub>3</sub>-CeO<sub>2</sub> (1.0, 3.0, 5.0, 7.5, and 10wt% of Ce) support was wetted by distilled water in a beaker in order to have high dispersion and to maximize the mass transfer of added metal salt (RuCl<sub>3</sub>\*XH<sub>2</sub>O) on the surface and the pores of the catalyst. The resulting solution is stirred for 1 h; after that it is heated at 60°C. The samples were dried at 120°C for 24 h and then calcined under air flow (60 ml/min) at 650°C for 4 h, with a heat rate of 2°C/min. Finally, the catalysts were reduced under H<sub>2</sub> (60 ml/min) at 400°C for 5 h, with a heat rate of 2°C/min. The synthesized monometallic catalysts will be named as RuAlIH, RuAlCe<sub>1</sub>IH, RuAlCe<sub>3</sub>IH, RuAlCe<sub>5</sub>IH, RuAlCe<sub>7.5</sub>IH, and RuAlCe<sub>10</sub>IH.

### 2.3 Synthesis of noble and base metal catalysts by deposition-precipitation

Deposition of gold into the modified supports was carried out by the method of deposition-precipitation using urea according to the procedure described below. Support powder (Al<sub>2</sub>O<sub>3</sub>, CeO<sub>2</sub>, Al<sub>2</sub>O<sub>3</sub>-CeO<sub>2</sub> (1wt%), Al<sub>2</sub>O<sub>3</sub>-CeO<sub>2</sub> (5wt%), Al<sub>2</sub>O<sub>3</sub>-CeO<sub>2</sub> (10wt%)) was first dispersed in distilled water. The temperature of the suspension was kept constant at 80°C and agitated with a magnetic stirrer. Secondly, the requisite quantity of chloroauric acid (HAuCl<sub>4</sub>) solution was added to the suspension, and the temperature was let to stabilize. Thirdly, 2.33 g of urea was added into the reactor vessel, and the suspension was stirred continuously for 16 h. The deposition was followed by centrifugation of the catalyst suspension in 50 ml tubes. The centrifugation was conducted three times. Separated water was decanted away, and the tube was refilled with distilled water after the first and the second centrifugations. Posterior the following separation and washing, the solid was collected and moved to a rotary evaporator and dried at 60°C in a water bath under vacuum. Final drying was done in an oven at 120°C overnight. All catalysts were calcined in air flow by heating them from room temperature up to 300°C for 4 h. The synthesized monometallic catalysts will be named as AuAlDPU, AuCeDPU, AuAlCe<sub>1</sub>DPU, AuAlCe<sub>5</sub>DPU, and AuAlCe<sub>10</sub>DPU.

The supported Ag nanoparticles were synthesized by DP with NaOH. The procedure was the same as the described for the gold synthesis by DP with urea, only that, instead of urea, NaOH was occupied, regulating solution's pH to 9. The synthesized monometallic catalysts will be named as AgCeDPNa, AgAlDPNa, AgAlCe<sub>1</sub>DPNa, AgAlCe<sub>3</sub>DPNa, AgAlCe<sub>5</sub>DPNa, AgAlCe<sub>7.5</sub>DPNa, and AgAlCe<sub>10</sub>DPNa. All the catalysts prepared are mentioned in **Table 1**.

### 2.4 Characterization of noble (Ru, Au, Ag) and base (Cu) metal nanoparticles supported

**Figure 1** shows the adsorption isotherms of the synthesized materials of RuAlIH and RuAlCe<sub>1</sub>IH. It was observed that both isotherms are of type IV, which were associated with capillary condensation in mesoporous catalysts, where the hysteresis loops indicated that the pores are well distributed.

For the catalysts of RuAlIH and RuAlCe<sub>1</sub>IH (the other TPR analyzes the rest of the catalysts not shown), **Figure 2** which displayed a main peak of 36–52°C was

Catalyst abbreviation	Synthesis method						Target molecule		
	One step			Two step			MTBE	ETBE	TAME
	Wet impregnation	Sol-gel	Wet impregnation with urea	Wet impregnation	Deposit-precipitation With urea	Deposit-precipitation With NaOH			
Cu <sub>5</sub> AlIH	X							x	x
Cu <sub>10</sub> AlIH	X							x	x
C <sub>15</sub> AlIH	X							x	x
Cu <sub>5</sub> AlSG,		x						x	x
Cu <sub>10</sub> AlSG		x						x	x
Cu <sub>15</sub> AlSG		x						x	x
Cu <sub>15</sub> AlSGp		x						x	x
Cu <sub>5</sub> AlIHU			x					x	x
Cu <sub>10</sub> AlIHU			x					x	x
Cu <sub>15</sub> AlIHU			x					x	x
Cu <sub>15</sub> AlIHp			x					x	x
RuAlIH				x			x		
RuAlCe <sub>1</sub> IH				x			x		
RuAlCe <sub>3</sub> IH				x			x		
RuAlCe <sub>5</sub> IH				x			x		
RuAlCe <sub>7.5</sub> IH				x			x		
RuAlCe <sub>10</sub> IH				x			x		
AuAlDPU					x		x		x
AuCeDPU					x		x		x

Catalyst abbreviation	Synthesis method						Target molecule		
	One step			Two step			MTBE	ETBE	TAME
	Wet impregnation	Sol-gel	Wet impregnation with urea	Wet impregnation	Deposit-precipitation With urea	Deposit-precipitation With NaOH			
AuAlCe <sub>1</sub> DPU					x		x		x
AuAlCe <sub>3</sub> DPU					x		x		x
AuAlCe <sub>5</sub> DPU					x		x		x
AuAlCe <sub>10</sub> DPU					x		x		x
AgCeDPNa						x	x		
AgAlDPNa						x	x		
AgAlCe <sub>1</sub> DPNa						x	x		
AgAlCe <sub>3</sub> DPNa						x	x		
AgAlCe <sub>5</sub> DPNa						x	x		
AgAlCe <sub>7.5</sub> DPNa						x	x		
AgAlCe <sub>10</sub> DPNa						x	x		

**Table 1.**

Lists the Cu, Ag, Au, and Ru catalysts supported on Al<sub>2</sub>O<sub>3</sub>, CeO<sub>2</sub>, and Al<sub>2</sub>O<sub>3</sub>-CeO<sub>2</sub>, tested in CWAO of fuel oxygenated (FO) with the operating conditions: T = 100°C, P(O<sub>2</sub>) = 10 bar, V<sub>Liq</sub> = 0.25 l, CFO = 1000 mg/l, C<sub>Cat</sub> = 1 g/l, and ω = 1000 rpm.

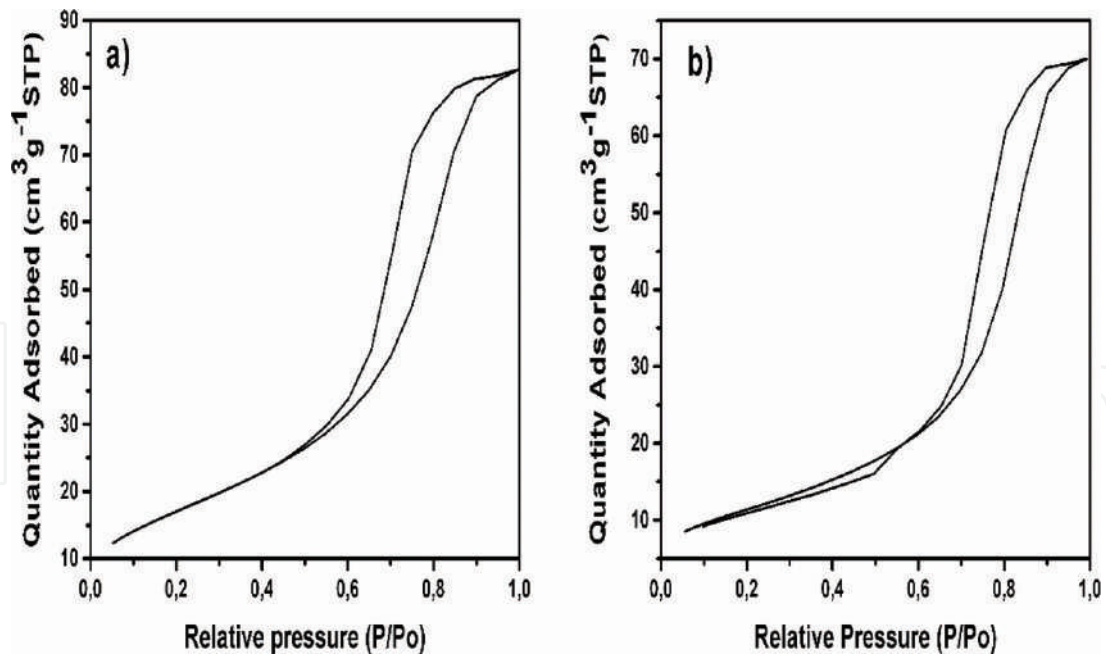


Figure 1.  
Adsorption isotherms of (a) RuAlIH and (b) RuAlCe<sub>1</sub>IH.

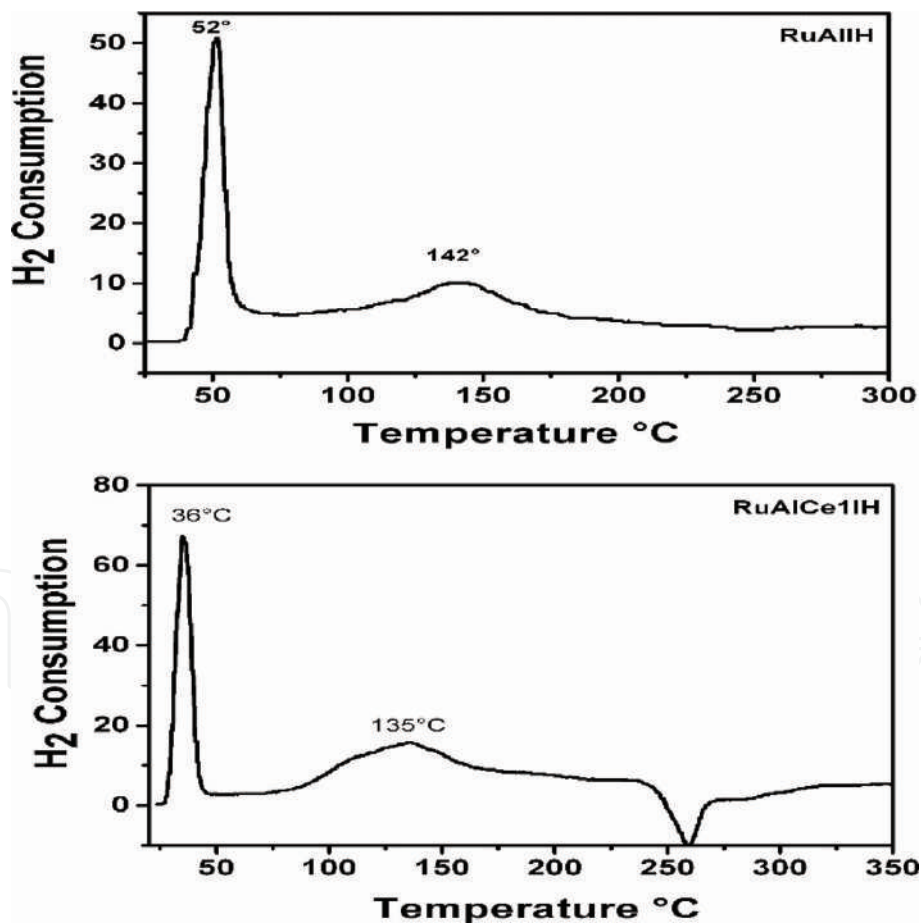


Figure 2.  
H<sub>2</sub>-TPR profiles of the catalysts RuAlIH and RuAlCe<sub>1</sub>IH.

observed which indicates that the reduction is carried out in that first peak, and it was attributed to the oxidation change of Ru from +2 to 0 (RuO) since it was the species that was reduced first. The second signal observed at 135–142°C was attributed to ruthenium oxide (RuO<sub>2</sub>), with an oxidation state of +4 which passes from +4 to +2 and subsequently to 0. On the other hand, the two peaks clearly observed in **Figure 2**

indicated that the ions of Ru existed in two different states to be reduced with hydrogen, meaning that at the end of the reduction, only the states +2 and 0 remain.

**Figure 3** corresponds to the diffraction patterns of the catalysts containing Au. It showed only signals corresponding to  $\text{Al}_2\text{O}_3$  and  $\text{CeO}_2$ , and only a decrease of the alumina signal was observed when the content of  $\text{Al}_2\text{O}_3$ - $\text{CeO}_2$  increases by 10%. The corresponding Au signals were not shown in this diffractogram due to the weight % in which the catalysts were prepared, and in XRD only the metal was observed at concentrations higher than 2 and sometimes 3%.

In **Figure 4**, the  $\text{H}_2$ -TPR profiles of the Au-supported catalysts revealed that the first reduction peaks (around  $50^\circ\text{C}$ ) appearing for all Au-supported catalysts corresponded to the highly dispersed Au peaks on the catalyst surface. This signal increased to values higher than  $50^\circ\text{C}$  in the case of the Au catalyst deposited in Ce which indicates a difference in the size of the particles (observed by TEM). The second peak (around  $100^\circ\text{C}$ ) was attributed to a second oxidation state of Au that interacts with Ce. This signal increased with the Ce content. This can be supported since in the AuAlDPU catalyst, this signal did not appear; however, it appeared in the AuCeDPU catalyst.

**Figure 5** shows the XRD for the copper catalysts prepared by wet impregnation method, in which  $\gamma$ - $\text{Al}_2\text{O}_3$  phase was seen as well as the intense signals that indicated the presence of  $\text{CuO}$ , and the boehmite, indicating that the metal was correctly dispersed in the three synthesized catalysts.

## 2.5. Catalytic evaluation (MTBE, ETBE, TAME)

### 2.5.1 Reaction conditions

The activity level tests of the catalysts synthesized in this study were carried out in a Parr batch 300 ml batch reactor, under the conditions of  $100^\circ\text{C}$ , 10 bar, and 1000 ppm of fuel oxygenated. In the standard procedure for a CWAO experiment,

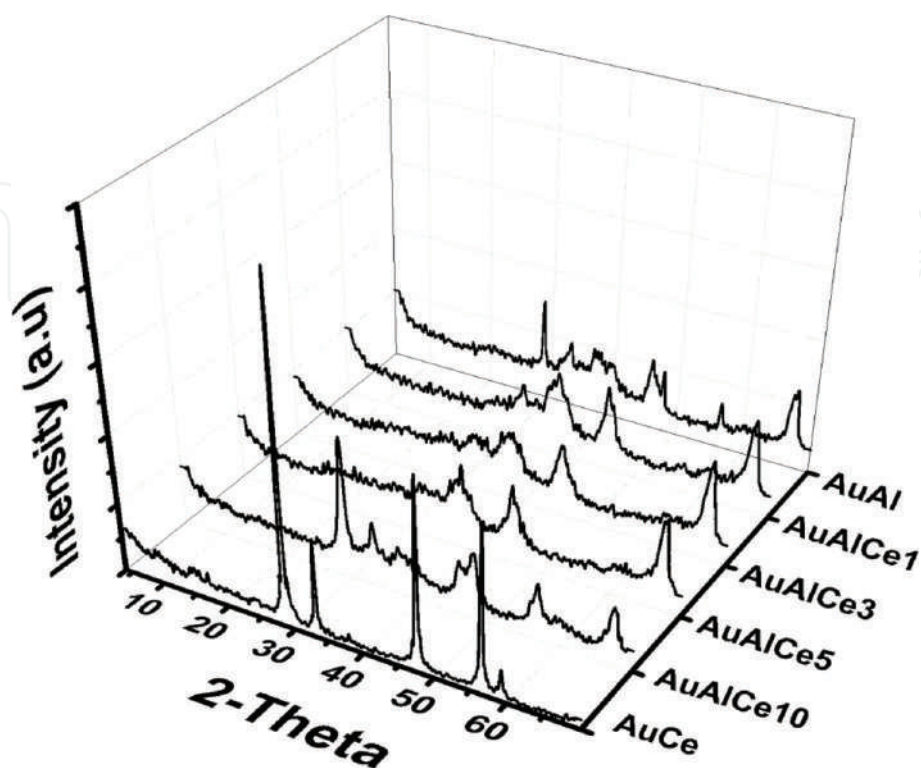


**Figure 3.**  
X-ray diffraction patterns of Au-supported catalysts.

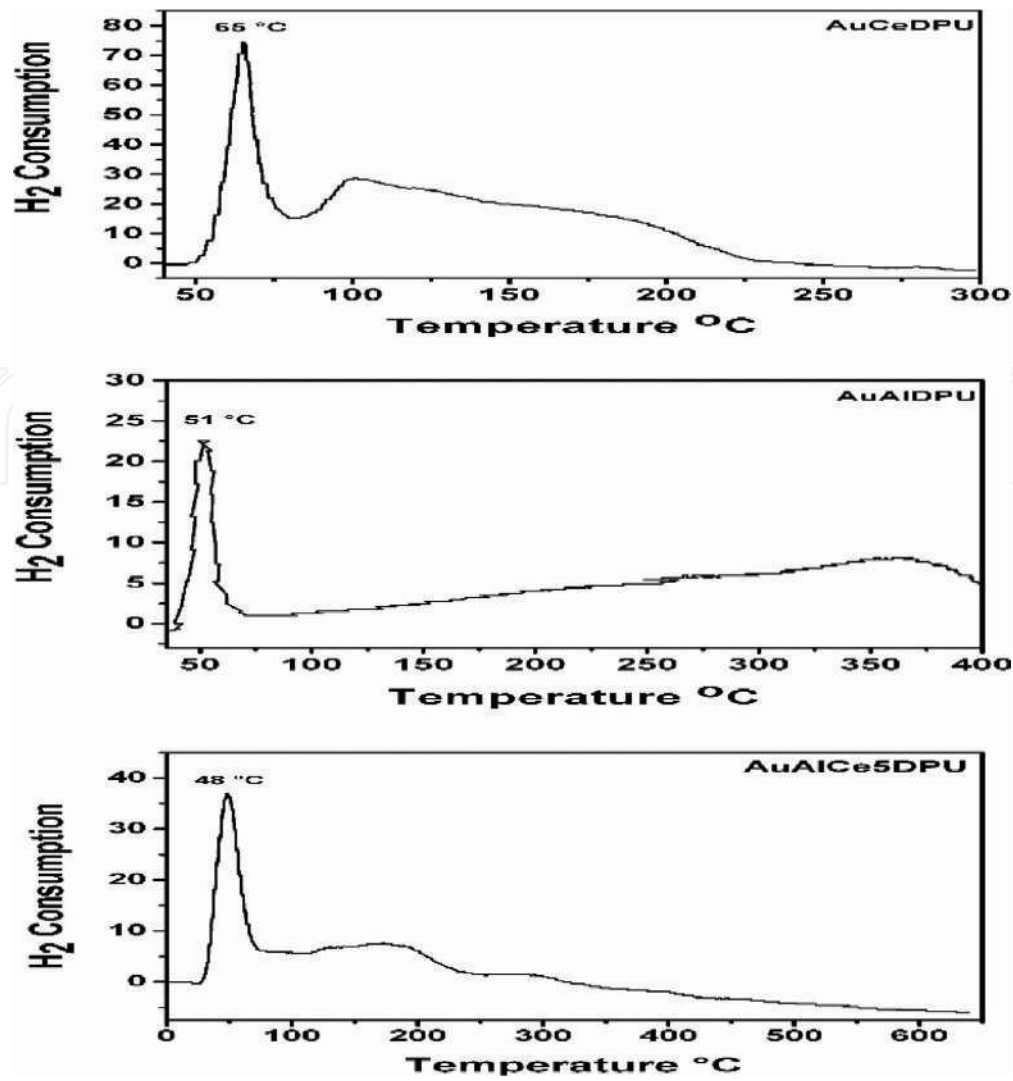


Figure 4.  
 $H_2$ -TPR of Au-supported catalysts.

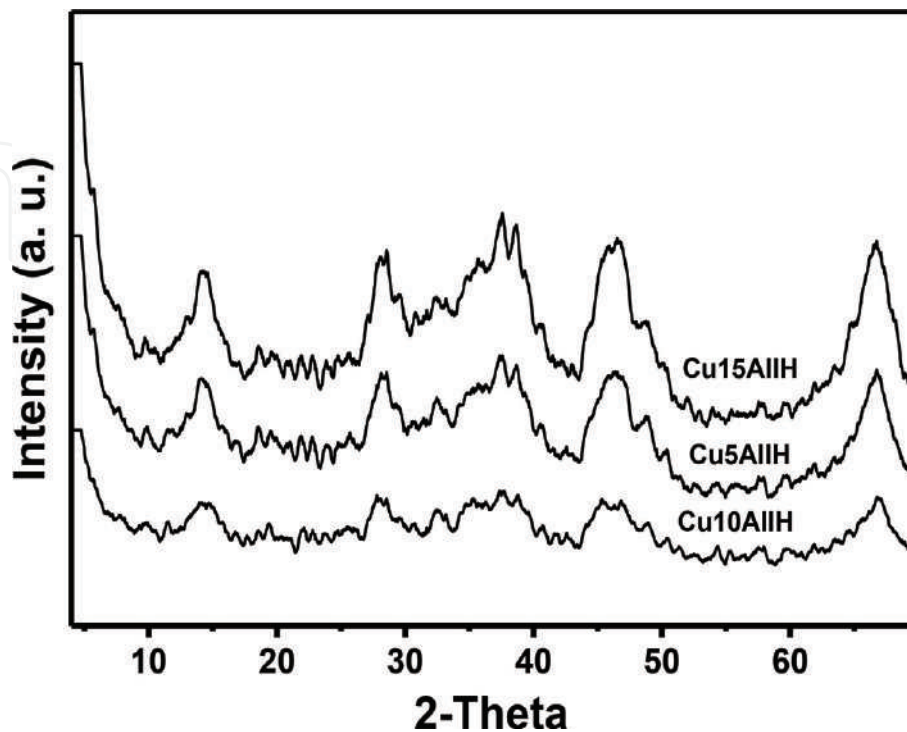


Figure 5.  
X-ray diffraction patterns for the Cu-supported catalysts synthesized by wet impregnation in a single step.

250 ml of fuel oxygenated solution were poured, and 0.25 g of catalyst were placed in the 300 ml reactor. When the selected temperature was reached, stirring was started at a maximum speed of 1000 rpm. This time was taken as the zero reaction time and the reaction duration was 60 min. These conditions were the same for all synthesized materials. The liquid samples were periodically removed from the reactor, then filtered to remove any catalyst particles, and finally analyzed by gas chromatography and total organic carbon (TOC).

With the following equation, the conversion values for total organic carbon and FO were determined at different times with intervals of 30 min up to 180 min of reaction:

$$X_{TOC} = \frac{TOC^0 - TOC^{60}}{TOC^0} \times 100 \quad (1)$$

$$X_{FO} = \frac{C_0 - C_{60}}{C_0} \times 100\% \quad (2)$$

where  $TOC^0$  is TOC at  $t = 0$  (ppm),  $C_0$  is FO concentration at  $t = 0$  (ppm),  $C_{60}$  is FO concentration at  $t = 1$  h of reaction (ppm), and  $TOC^{60}$  is TOC at  $t = 1$  h of reaction (ppm).

The initial rate ( $r_i$ ) was calculated from FO conversion depending on time, using the following equation:

$$r_i = \left( \frac{\Delta_{FO}(\%)}{\Delta t m_{cat}} \right) ([contaminant]_i) \quad (3)$$

where  $\frac{\Delta_{FO}(\%)}{\Delta t}$  is the initial slope of the conversion curve,  $[contaminant]_i$  = initial FO concentration, and  $m_{cat}$  = catalyst mass (g<sub>cat</sub>/l).

So the selectivity was calculated according to the following equation:

$$S_{CO_2} = \frac{X_{TOC}}{X_{FO}} \times 100 \quad (4)$$

### 2.5.2. Degradation of MTBE by catalytic wet air oxidation over noble and base metals

This research studied the degradation of the fuel oxygenated MTBE through CWAO occupying Ru, Au, and Ag as the catalysts, which will be responsible for mineralizing the pollutant.

**Figure 6** shows the results of the catalytic activity for CWAO of MTBE with the sets of catalysts Ru, Au, and Ag. The best activity for the set of ruthenium-supported catalysts was for the one named RuAlCe<sub>1</sub>IH, since it presented a 68% conversion of MTBE and a 63% degradation of TOC; the most favorable results for this particular catalyst were attributed to a particle size of 9 nm measured by TEM, and to the contribution of ceria, due to the oxygen storage capacity phenomenon. Ceria is known for having the capacity to exchange oxygen, through its vacancies of oxygen, which promotes the increase of selectivity in all cases with the Ru-synthesized catalysts from a chlorinated salt, by the formation of a species of type Ce<sup>4+</sup> – O<sup>2-</sup> – M<sup>+</sup>, contributing to improve the reducibility of ruthenium.

With respect to the Au-supported catalysts, AuAlCe<sub>5</sub>DPU was the one that stood out for its catalytic performance in comparison to the rest of its counterparts. AuAlCe<sub>5</sub>DPU reached a maximum of 73% MTBE conversion and a TOC degradation of 72%, indicating that this catalyst was efficient both to have a good

conversion and to transform to CO<sub>2</sub>. This behavior was explained by the fact of presenting the best distribution of particles on the surface of the catalyst, according to the TEM analysis, and confirmed by TPR. The largest amount of active particles for this catalyst was below 2 nm. It was observed that the other catalysts had a similar activity attributable to the distribution of particle sizes ranging between 2 and 10 nm. According to the performed analysis, well-dispersed Au nanoparticles and the oxidation state of Au play an important role in this type of oxide-reduction reactions. The excess of CeO<sub>2</sub> does not allow a good selectivity toward CO<sub>2</sub> since it interferes in the exchange of O<sub>2</sub> at the time of oxidation, giving an excess of oxygen that causes the metal particle to change its oxidation state on the surface of the catalyst and confirming the theory made by Imamura et al. [26] that a balance of metal particles in oxidized and reduced state is needed to obtain satisfactory results in terms of activity and selectivity; this theory is fulfilled in molecules that are strongly adsorbed on the surface of the catalyst such as acetic acid, and according to this study, this principle can be also applied with MTBE.

The results of the catalytic activity for CWAO of MTBE for the set of silver catalysts indicated that the best conversion obtained corresponds to the AgCeDPNa catalyst with 66%, due to the presence of CeO<sub>2</sub>. In this case, we can only mention an effect of CeO<sub>2</sub> because the particle sizes obtained by HRTEM and TPD-CO revealed different distributions but did not significantly impact the catalytic activity. This effect has been explained by several researchers as the formation of a bridge M-O-Ce where M means silver metal. The AgCeDPNa catalyst was the one that has a better behavior toward mineralizing CO<sub>2</sub> due to the oxide-reducing properties of this support. However, it was observed that the catalyst with 5% of CeO<sub>2</sub> has a very close TOC value with respect to the AgCeDPNa catalyst. In this case, the effect between the particle size, the activity, and the selectivity toward CO<sub>2</sub> was not possible to distinguish because, as the HRTEM histograms showed, the range of sizes was

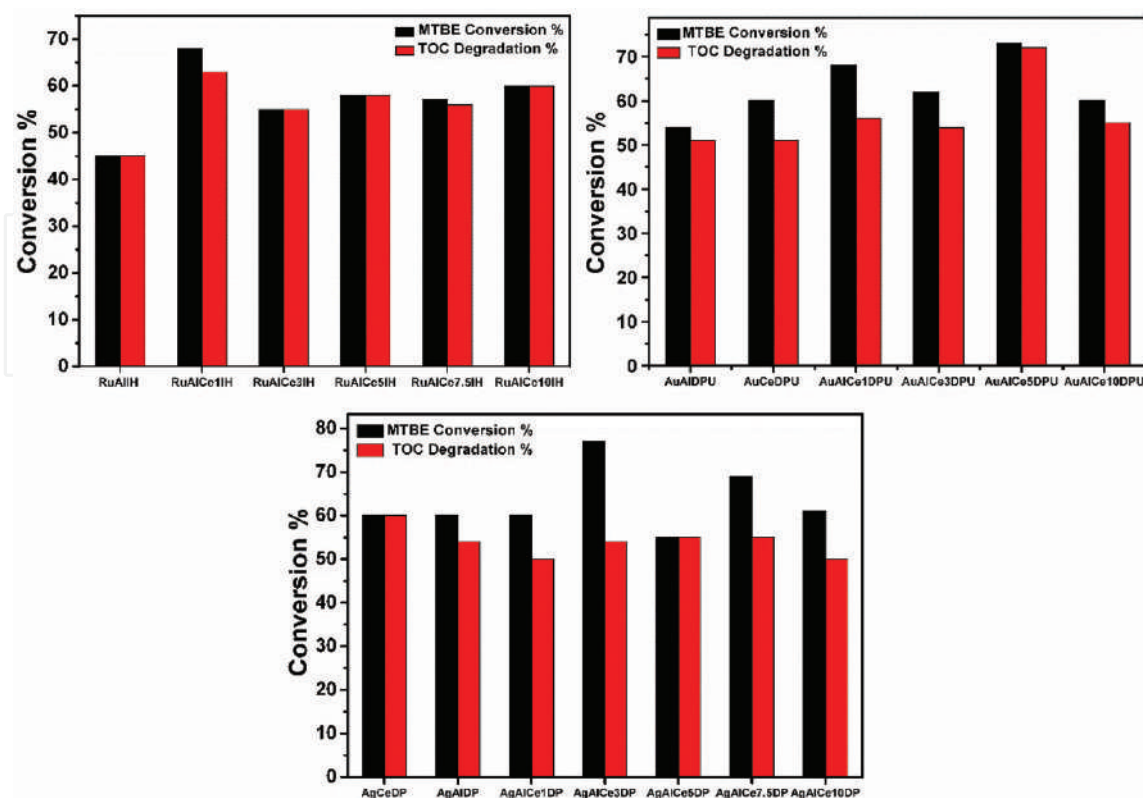


**Figure 6.** MTBE conversion and TOC degradation, at 100°C and 10 oxygen bar over Ru-, Au-, and Ag-supported catalysts.

very broad in all cases; nonetheless, the effect of CeO<sub>2</sub> appeared in the activity and also in the selectivity. Imamura proposed a theory stating that a balance of metal particles in oxidized and reduced state is needed to obtain satisfactory results in terms of activity and selectivity, which is observed here by TPR of H<sub>2</sub> in the case of AgCeDPNa catalyst; Ag particles remain oxidized even with the passage of H<sub>2</sub> which makes them more selective toward CO<sub>2</sub>. It is not possible in this case to account for the proportion of Ag<sup>+</sup>/AgO particles because this can only be done by XPS, a very expensive technique and not available in this case; however, it can be concluded that, in terms of activity, the optimal catalyst is the one that only contains ceria.

### 2.5.3. Degradation of ETBE by catalytic wet air oxidation over noble and base metals

We also analyzed the degradation process of the ETBE molecule through CWAO using Cu synthesized by three different synthesis methods, with the main characteristic of being carried out in a single step. The aim of the application of these methods is to avoid the leaching of the metal, which has occurred in other previous experiments by different investigators, after having passed a certain time of the reaction.

The analysis results of the ETBE-treated solutions by CWAO are presented in **Table 2**; for each of the three synthesis methods of the Cu catalysts, Cu<sub>10</sub>AlSG and Cu<sub>10</sub>AlIHU catalysts were more active, obtaining 88 and 89% ETBE conversion, respectively, after 1 h of oxidation. But the highest values for TOC degradation were obtained with the catalysts prepared by sol-gel method, as Cu<sub>5</sub>AlSG reached 84% and Cu<sub>10</sub>AlSG 89%. This last result confirmed that Cu catalysts synthesized by sol-gel are more effective catalysts for the mineralization process, which allows to degrade the organic matter, coming from the contaminant present, by almost 90% until obtaining CO<sub>2</sub> in the treated solutions. In addition, we can affirm that the optimum percentage of Cu was 10%, as well as the commercial catalyst used for this type of reactions and reported in the literature.

Another discovery in this study with copper nanoparticles was realized by measuring copper concentration through atomic absorption in the ETBE-treated solutions, since no copper concentrations were obtained, particularly in the catalysts prepared by sol-gel method, opposite situation for the other catalysts prepared

Catalyst	ETBE conversion %	% TOC	SCO <sub>2</sub>
Cu <sub>5</sub> AlIH	76	81	100
Cu <sub>10</sub> AlIH	66	82	100
Cu <sub>15</sub> AlIH	72	80	100
Cu <sub>5</sub> AlSG	82	84	100
Cu <sub>10</sub> AlSG	88	89	100
Cu <sub>15</sub> AlSG	80	78	97
Cu <sub>15</sub> AlSGp	78	74	95
Cu <sub>5</sub> AlIHU	71	59	83
Cu <sub>10</sub> AlIHU	89	79	89
Cu <sub>15</sub> AlIHU	86	81	94
Cu <sub>15</sub> AlIHp	80	69	86

**Table 2.**

ETBE conversion, TOC and SCO<sub>2</sub> at 100°C and 10 bar of pressure during 1 h of reaction with one of [ETBE]<sub>0</sub> = 1000 ppm.

by wet impregnation and wet impregnation with urea. Therefore, we can encapsulate the copper in the alumina, by sol-gel method, thus avoiding contamination by the metal, leaching, and, in turn, obtaining an improvement in the catalytic performance of the metal.

#### 2.5.4. Degradation of TAME by catalytic wet air oxidation over noble and base metals

Another series of experiments was conducted under the same conditions described below over Cu synthesized in three different methods and Au-supported catalyst but in this experiments with TAME as a target molecule by CWAO.

**Table 3** presents the analysis results of the treated solutions of TAME by CWAO; for each of the three synthesis methods of the Cu catalysts, the catalysts of Cu<sub>15</sub>AlSG and Cu<sub>10</sub>AlIHU were more active, obtaining 78% of TAME conversion, for both catalysts after 1 h of reaction. But the highest values for TOC degradation were obtained with the catalysts prepared by sol-gel method; Cu<sub>15</sub>AlSG reached 78% and Cu<sub>10</sub>AlIHU 75%. These results sustained that the Cu catalysts synthesized by sol-gel were more effective catalysts for TAME mineralization process, which allows them to degrade the organic matter, coming from the existing contaminant, by almost 80% in the treated solutions.

The results of the catalytic activity for TAME CWAO in Au-supported catalysts are shown in **Figure 7**. It was observed that the best activity happened with the catalyst at AuAlCe<sub>10</sub>DPU with 80% conversion of TAME, although all the remaining catalysts showed good activity except for the catalyst with AuAlCe<sub>1</sub>DPU; this could be explained by the fact that this molecule may not be very sensitive to particle size due to its structure.

**Figure 7** also shows the abatement of TOC of the supported Au catalysts; as can be seen the best carbon transformation toward CO<sub>2</sub> was obtained for the AuAlCe<sub>3</sub>DPU catalyst, with a 77% conversion, and for the AuCeDPU catalyst with 80%, although all the remaining catalysts showed a remarkable performance, without exceeding these, except for AuAlCe<sub>1</sub>DPU.

**Table 4** shows the selectivity to CO<sub>2</sub>, and we can say that the supported Au catalysts containing Ce 5 and 10% were the least selective to CO<sub>2</sub>. This is because there is

Catalyst	TAME conversion %	TOC	SCO <sub>2</sub>
Cu <sub>5</sub> AlIH	72	68	93
Cu <sub>10</sub> AlIH	68	61	89
Cu <sub>15</sub> AlIH	77	75	98
Cu <sub>5</sub> AlSG	73	68	94
Cu <sub>10</sub> AlSG	72	68	95
Cu <sub>15</sub> AlSG	78	78	100
Cu <sub>15</sub> AlSGp	70	41	59
Cu <sub>5</sub> AlIHU	49	64	100
Cu <sub>10</sub> AlIHU	78	75	95
Cu <sub>15</sub> AlIHU	66	62	95
Cu <sub>15</sub> AlIHp	69	34	50

**Table 3.** TAME conversion, TOC degradation, and SCO<sub>2</sub> at 100°C and 10 bar of pressure during 1 h of reaction with one of [TAME]<sub>0</sub> = 1000 ppm.

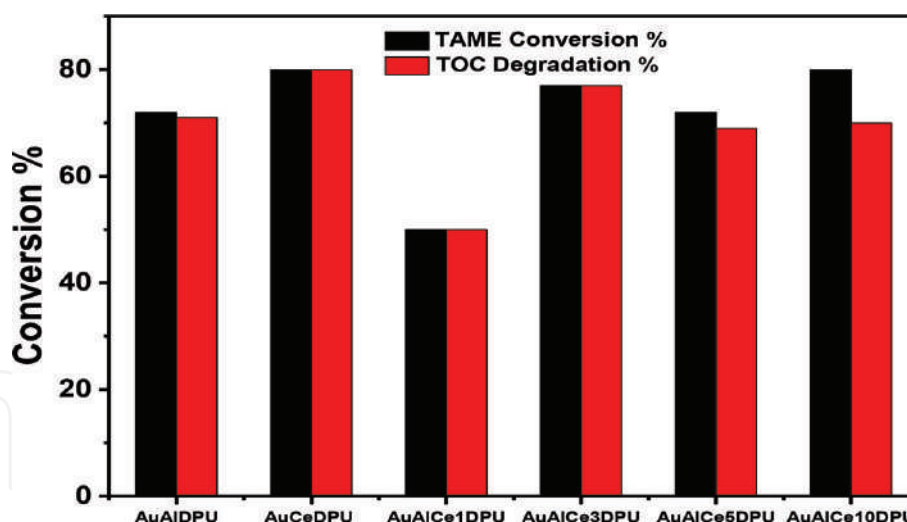


**Figure 7.** TAME conversion and TOC degradation % at 100°C and 10 bar over Au-supported catalysts.

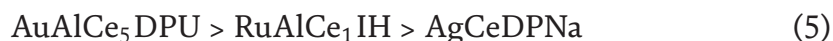
Catalysts	SCO <sub>2</sub>
AuAlDPU	99
AuCeDPU	100
AuAlCe <sub>1</sub> DPU	100
AuAlCe <sub>3</sub> DPU	100
AuAlCe <sub>5</sub> DPU	96
AuAlCe <sub>10</sub> DPU	88

**Table 4.** TAME selectivity at 100°C over Au-supported catalysts.

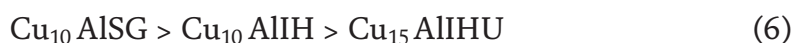
a poisoning by CeO<sub>2</sub> that affects the selectivity when it is in excess due to the interaction of M-Ce-O; this case shows that the optimal percentage of CeO<sub>2</sub> for the TAME is 3%. It is important to note that the AuAlCe<sub>3</sub>DPU catalyst is equally active and selective to the AuCeDPU catalyst, so the alumina-ceria support with low concentrations of CeO<sub>2</sub> is presented as an alternative for the wet oxidation process of TAME.

### 3. Conclusions

This study concludes that the catalytic activity for MTBE oxidation of catalysts Ru, Au, and Ag, supported on Al<sub>2</sub>O<sub>3</sub>, CeO<sub>2</sub>, and Al<sub>2</sub>O<sub>3</sub>-CeO<sub>2</sub>, synthesized by wet impregnation methods and DP with NaOH and urea, in two steps, is classified as follows:



In addition, the catalytic activity for the oxidation of target molecule ETBE on Cu catalysts supported on Al<sub>2</sub>O<sub>3</sub>, synthesized by three different methods in a single step, is classified as follows:



The catalytic activity for TAME oxidation using Copper catalysts supported on Al<sub>2</sub>O<sub>3</sub>, synthesized by three different methods in a single step and Au supported on

Al<sub>2</sub>O<sub>3</sub>, CeO<sub>2</sub> and Al<sub>2</sub>O<sub>3</sub>-CeO<sub>2</sub> synthesized by DP with urea in two steps, is classified as follows:



## Acknowledgements

Authors thank the National Council for Science and Technology (CONACYT) for financing the project 132648; thanks to the Universidad Juárez Autónoma de Tabasco for PFCE-DACB project and PRODEP program.

## Conflict of interest

Authors declare no conflicts of interest.

## Author details

Zenaida Guerra Que, José Gilberto Torres Torres\*, Ignacio Cuauhtémoc López, Juan C. Arévalo Pérez, Adrian Cervantes Uribe, Hermicenda Pérez Vidal, Alejandra E. Espinosa de los Monteros Reyna, José G. Pacheco Sosa, María A. Lunagómez Rocha and Cecilia Sánchez Trinidad  
Laboratory of Catalytic Nanomaterials Applied to the Development of Energy Sources and Environmental Remediation, Applied Science and Technology Research Center of Tabasco (CICTAT), DACB, Juarez Autonomous University of Tabasco, Tabasco, México

\*Address all correspondence to: [gilberto.torres@ujat.mx](mailto:gilberto.torres@ujat.mx)

## IntechOpen

© 2019 The Author(s). Licensee IntechOpen. This chapter is distributed under the terms of the Creative Commons Attribution License (<http://creativecommons.org/licenses/by/3.0>), which permits unrestricted use, distribution, and reproduction in any medium, provided the original work is properly cited. 

## References

- [1] Awad OI, Mamat R, Ibrahim TK, Hammid AT, Yusri IM, Hamidi MA, et al. Overview of the oxygenated fuels in spark ignition engine: Environmental and performance. *Renewable and Sustainable Energy Reviews*. 2018;**91**:394-408. DOI: 10.1016/j.rser.2018.03.107
- [2] McGregor D. Fuel Oxygenates. *Encyclopedia of Toxicology*. 3rd ed. Vol 2; USA: Academic Press, Elsevier Inc; 2014. pp. 671-681. ISBN: 9780123864543. DOI: 10.1016/b978-0-12-386454-3.00025-7
- [3] Cuauhtémoc I, Del Angel G, Torres G, Navarrete J, Angeles-Chavez C, Padilla JM. Synthesis and characterization of Rh/Al<sub>2</sub>O<sub>3</sub>-CeO<sub>2</sub> catalysts: Effect of the Ce<sup>4+</sup>/Ce<sup>3+</sup> ratio on the MTBE removal. *Journal of Ceramic Processing Research*. 2009;**10**:512-520
- [4] Bergendahl JA, Thies TP. Fenton's oxidation of MTBE with zero-valent iron. *Water Research*. 2004;**38**:327-334. DOI: 10.1016/j.watres.2003.10.003
- [5] Mehrjouei M, Müller S, Möller D. Decomposition kinetics of MTBE, ETBE and, TAEE in water and wastewater using catalytic and photocatalytic ozonation. *Journal of Molecular Catalysis A: Chemical*. 2014;**386**:61-68. DOI: 10.1016/j.molcata.2014.02.014
- [6] Bartling J, Esperschütz J, Wilke BM, Schloter M. ETBE (ethyl tert butyl ether) and TAME (tert amyl methyl ether) affect microbial community structure and function in soils. *Journal of Hazardous Materials*. 2011;**187**: 488-494. DOI: 10.1016/j.jhazmat.2011.01.058
- [7] Cuauhtémoc I, Del Angel G, Torres G, Bertin V. Catalytic wet air oxidation of gasoline oxygenates using Rh/ $\gamma$ -Al<sub>2</sub>O<sub>3</sub> and Rh/ $\gamma$ -Al<sub>2</sub>O<sub>3</sub>-CeO<sub>2</sub> catalysts. *Catalysis Today*. 2008;**133-135**:588-593. DOI: 10.1016/j.cattod.2008.02.006
- [8] Cuauhtémoc I, Del AG, Torres G, Angeles-chavez C, Navarrete J, Padilla JM. Enhancement of catalytic wet air oxidation of tert-amyl methyl ether by the addition of Sn and CeO<sub>2</sub> to Rh/Al<sub>2</sub>O<sub>3</sub> catalysts. *Catalysis Today*. 2011;**166**: 180-187. DOI: 10.1016/j.cattod.2010.11.100
- [9] Kasprzyk-Hordern B, Andrzejewski P, Dabrowska A, Czaczyk K, Nawrocki J. MTBE, DIPE, ETBE and TAME degradation in water using perfluorinated phases as catalysts for ozonation process. *Applied Catalysis B: Environmental*. 2004;**51**:51-66. DOI: 10.1016/j.apcatb.2004.02.004
- [10] Sun Y, Zhang Y, Quan X. Treatment of petroleum refinery wastewater by microwave-assisted catalytic wet air oxidation under low temperature and low pressure. *Separation and Purification Technology*. 2008;**62**: 565-570. DOI: 10.1016/j.seppur.2008.02.027
- [11] Fathy NA, El-Khouly SM, Hassan NA, Awad RMS. Free- and Ni-doped carbon xerogels catalysts for wet peroxide oxidation of methyl orange. *Journal of Water Process Engineering*. 2017;**16**:21-27. DOI: 10.1016/j.jwpe.2016.11.005
- [12] Redel-Macías MD, Pinzi S, Leiva-Candia DE, López I, Dorado MP. Ternary blends of diesel fuel oxygenated with ethanol and castor oil for diesel engines. *Energy Procedia*. 2017;**142**:855-860. DOI: 10.1016/j.egypro.2017.12.137
- [13] Abasaeed AE, Al-Fatesh AS, Naeem MA, Ibrahim AA, Fakeeha AH.

Catalytic performance of CeO<sub>2</sub> and ZrO<sub>2</sub> supported Co catalysts for hydrogen production via dry reforming of methane. *International Journal of Hydrogen Energy*. 2015; **40**(21):6818-6826. DOI: 10.1016/j.ijhydene.2015.03.152

[14] Cozzarelli IM, Mckelvie JR, Baehr AL. Volatile Hydrocarbons and Fuel Oxygenates. *Treatise on Geochemistry*. 2nd ed. Vol 11, 12. Oxford: Elsevier; 2014. pp. 439-480. DOI: 10.1016/b978-0-08-095975-7.00912-8

[15] Levchuk I, Bhatnagar A, Sillanpää M. Overview of technologies for removal of methyl tert-butyl ether (MTBE) from water. *Science of the Total Environment*. 2014; **476-477**:415-433. DOI: 10.1016/j.scitotenv.2014.01.037

[16] Van Afferden M, Rahman KZ, Mosig P, et al. Remediation of groundwater contaminated with MTBE and benzene: The potential of vertical-flow soil filter systems. *Water Research*. 2011; **45**:5063-5074. DOI: 10.1016/j.watres.2011.07.010

[17] Massa A, Hernández S, Ansaloni S, Castellino M, Russo N, Fino D. Enhanced electrochemical oxidation of phenol over manganese oxides under mild wet air oxidation conditions. *Electrochimica Acta*. 2018; **273**:53-62. DOI: 10.1016/j.electacta.2018.03.178

[18] Van Afferden M, Rahman KZ, Mosig P, De Biase C, Thullner M, Oswald SE, et al. Remediation of groundwater contaminated with MTBE and benzene: The potential of vertical-flow soil filter systems. *Water Research*. 2004; **38**(16):5063-5074. DOI: 10.1016/j.watres.2011.07.010

[19] Sutherland J, Adams C, Kekobad J. Treatment of MTBE by air stripping, carbon adsorption, and advanced

oxidation: Technical and economic comparison for five groundwaters. *Water Research*. 2004; **38**:193-205. DOI: 10.1016/j.watres.2003.09.008

[20] Tsoncheva T, Ivanova R, Henych J, Dimitrov M, Kormunda M, Kovacheva D, et al. Effect of preparation procedure on the formation of nanostructured ceria—Zirconia mixed oxide catalysts for ethyl acetate oxidation: Homogeneous precipitation with urea vs template-assisted hydrothermal synthesis. *Applied Catalysis A: General*. 2015; **502**:418-432. DOI: 10.1016/j.apcata.2015.05.034

[21] Roy B, Martinez U, Loganathan K, Datye AK, Leclerc CA. Effect of preparation methods on the performance of Ni/Al<sub>2</sub>O<sub>3</sub> catalysts for aqueous-phase reforming of ethanol: Part I-catalytic activity. *International Journal of Hydrogen Energy*. 2012; **37**:8143-8153. DOI: 10.1016/j.ijhydene.2012.02.056

[22] Benito P, Gregori M, Andreoli S, Fornasari G, Millefanti S, Ospitali F, et al. Role of the preparation method on properties of Pd/Cu-MCM-41 hydrodechlorinating catalysts. *Catalysis Today*. 2014; **235**:134-143. DOI: 10.1016/j.cattod.2014.01.034

[23] Manzoli M, Menegazzo F, Signoretto M, Cruciani G, Pinna F. Effects of synthetic parameters on the catalytic performance of Au/CeO<sub>2</sub> for furfural oxidative esterification. *Journal of Catalysis*. 2015; **330**:465-473. DOI: 10.1016/j.jcat.2015.07.030

[24] Levec J, Pintar A. Catalytic wet-air oxidation processes: A review. *Catalysis Today*. 2007; **124**(3-4):172-184. DOI: 10.1016/j.cattod.2007.03.035

[25] Kim SK, Kim KH, Ihm SK. The characteristics of wet air oxidation of phenol over CuOx/Al<sub>2</sub>O<sub>3</sub> catalysts:

Effect of copper loading. *Chemosphere*.  
2007;**68**:287-292. DOI: 10.1016/j.  
chemosphere.2006.12.080

[26] Hosokawa S, Kanai H, Utani K,  
Taniguchi YI, Saito Y, Imamura S. State  
of Ru on CeO<sub>2</sub> and its catalytic activity  
in the wet oxidation of acetic acid.

*Applied Catalysis B: Environmental*.  
2003;**45**:181-187. DOI: 10.1016/  
S0926-3373(03)00129-2

IntechOpen

# We are IntechOpen, the world's leading publisher of Open Access books Built by scientists, for scientists

6,300

Open access books available

171,000

International authors and editors

190M

Downloads

Our authors are among the

154

Countries delivered to

TOP 1%

most cited scientists

12.2%

Contributors from top 500 universities



WEB OF SCIENCE™

Selection of our books indexed in the Book Citation Index  
in Web of Science™ Core Collection (BKCI)

Interested in publishing with us?  
Contact [book.department@intechopen.com](mailto:book.department@intechopen.com)

Numbers displayed above are based on latest data collected.  
For more information visit [www.intechopen.com](http://www.intechopen.com)



# Removal of Cr(VI) from Waters by Multi-Walled Carbon Nanotubes: Optimization and Kinetic Investigations

*Francisco J. Alguacil and Félix A. Lopez*

## Abstract

The adsorption of chromium(VI) from aqueous solutions onto multi-walled carbon nanotubes (MWCNTs) has been investigated under various experimental conditions of initial metal concentration, agitation speed, aqueous pH, temperature and adsorbent dosage to assess the equilibrium and kinetic parameters. It was found that the kinetic data were fitted with the pseudo-first- and pseudo-second-order models, whereas the chromium(VI) adsorption data were fitted with the Langmuir and Freundlich equilibrium models to give the characteristic parameters of each model. According with the evaluation, both isotherm models are useful to represent the measured adsorption data. The adsorption of chromium(VI) is also dependent on the temperature, and the corresponding thermodynamic parameters including  $\Delta H^\circ$ ,  $\Delta G^\circ$  and  $\Delta S^\circ$  were estimated from the experimental data, indicating the exothermic and non-spontaneous nature of the metal adsorption onto the MWCNTs. Chromium(VI) desorption was investigated by the use of aqueous hydrazine sulfate solutions.

**Keywords:** chromium(VI), multi-walled carbon nanotubes, adsorption, desorption, kinetics

## 1. Introduction

Despite its toxic character, chromium(VI) is widely used in various industries, being its recovery from the corresponding liquid effluents a primary target before their discharge to natural waters. Several technologies have found application to remove and/or recover chromium(VI) from these process wastes: pseudo-emulsion strip dispersion pertraction [1, 2], adsorption onto activated carbons [3], liquid-liquid extraction [4], biomass adsorption [5, 6], adsorption onto natural zeolites [7], adsorption onto phosphates [8], ion exchange [9] and electro-assisted and photo-assisted technologies [10]. Among them, adsorption onto carbon nanotube (CNT) technology could be competitive when the metal is present at low concentrations in the aqueous solution. Various carbon nanotubes configurations can be found, being the most commonly used the single-walled carbon nanotubes (SCNTs) and multi-walled carbon nanotubes (MWCNTs) configurations, together with functionalized multi-walled carbon nanotubes. In either configuration, and

after the metal adsorption, a subsequent operation or elution is needed in order to recover the metal to a solution where it is concentrated and purified, and thus it can be conveniently recovered or even recycled to the original industrial process.

A number of examples using these CNTs for chromium(VI) recovery from aqueous solutions can be found in the literature. Naghizadeh [11] investigated the adsorption efficiency of activated carbon and multi-walled carbon nanotubes respect to cadmium(II) and chromium(VI) in the 3–12 pH range. Whereas both adsorbents presented high metal adsorption capacities over the whole pH range investigated, the experimental results indicated that MWCNTs had a greater potential for the removal of chromium(VI) and cadmium(II) from aqueous solutions than activated carbon. In an investigation by [12], oxidized (–COOH) multi-walled carbon nanotubes were used to remove Cr(VI) (hazardous element) and Au(III) (valuable element), from aqueous solutions. Experiments were performed in order to investigate the influence of different variables on the adsorption kinetics, i.e., the stirring speed (250–2000 min<sup>-1</sup>) and adsorbent dosage (0.25–1.5 g/L) in the case of chromium(VI) as well as temperature (20–60°C) and HCl (0.1–10 M) concentration in the case of gold(III). The performance of these carbon nanotubes was excellent in the removal of both elements, presented as the anions HCrO<sub>4</sub><sup>-</sup> and AuCl<sub>4</sub><sup>-</sup>, from the aqueous solutions.

Anastopoulos et al. [13] reviewed the removal of chromium(III) and (VI) from aqueous solutions by carbon nanotubes. In both cases, the pH of the solution seemed to control the adsorption process, with a maximum adsorption of Cr(VI) occurring at pH 1–4 (in the case of Cr(III), the above occurs at pH values of 5–8). Furthermore, it is stated that most of the investigations are reported using non-real wastewater, conditions that very often are not repeated in real wastewaters. Xing et al. [14] presented a novel remediation protocol for Cr(VI) featured with high-capacity adsorption and electrochemical regeneration of the adsorbent. In their study, MWCNTs modified carbon cloth (CC) is used as a useful carrier for electrodepositing polypyrrole (PPy) film and the resultant nanocomposite CC-MWCNTs-PPy is used as an adsorbent with high adsorption capacity and stability. CC-MWCNTs-PPy is electrically regenerated to reduce secondary wastes.

In the present work, results obtained for the adsorption of chromium(VI) using multi-walled carbon nanotubes are presented. Several variables that could affect the adsorption process, such as the stirring speed of the aqueous solution, metal concentration and adsorbent dosage, temperature, etc., are investigated. Several equilibrium, kinetics and thermodynamic parameters are also reported. The desorption of the Cr(VI)-loaded MWCNTs is accomplished using aqueous solutions of hydrazine sulfate.

## 2. Methods

### 2.1 Reactives and experimental procedure

The multi-walled carbon nanotubes were obtained from Fluka and were used without further purification; the main characteristics of the adsorbent are given in **Table 1**, with further characteristics (i.e., Raman data) of them published elsewhere [15]. The characteristics of other adsorbent-ion exchangers used in this investigation were described elsewhere: Dowex 1x8 resin [16], oxidized MWCNTs [12] and activated carbon [17].

Stock Cr(VI) solutions were prepared by dissolving K<sub>2</sub>Cr<sub>2</sub>O<sub>7</sub> (Merck) in distilled water. All other chemicals were of AR grade.

Type	Multi-walled
Melting range	3652–3697°C
Density	2.1 g/mL
Appearance	Dust
Purity	≥98% carbon basis
Dimensions	10 ± 1 nm external diameter
Maximum adsorption	4.5 ± 0.5 nm internal diameter
BET	3–6 μm (length)
	1295 cm <sup>3</sup> /g
	263 m <sup>2</sup> /g

**Table 1.**  
 Characteristics of the multi-walled carbon nanotubes.

Metal adsorption (and elution) studies were carried out in a glass reactor provided for mechanical shaking. Metal adsorption (or elution) was determined by monitoring concentration by AAS in the aqueous solution as a function of time, whereas the metal concentration in the adsorbent was calculated by mass balance.

## 2.2 Modeling of kinetic adsorption

### 2.2.1 Pseudo-first-order model

The pseudo-first-order equation [18] used in this work can be expressed accordingly with the next equation:

$$\ln([Cr]_{c,e} - [Cr]_{c,t}) = \ln[Cr]_{c,e} - k_1 t \quad (1)$$

where  $[Cr]_{c,t}$  and  $[Cr]_{c,e}$  are the chromium concentrations in the nanotubes at equilibrium and at an elapsed time, respectively,  $t$  is the time and  $k_1$  is the constant related to this model.

### 2.2.2 Pseudo-second-order model

In this model, the equation used is

$$\frac{t}{[Cr]_{c,t}} = \frac{1}{k_2 [Cr]_{c,e}^2} + \frac{t}{[Cr]_{c,e}} \quad (2)$$

In this case,  $k_2$  is the constant related to this model.

## 2.3 Modeling the rate law

Three possible adsorption mechanisms had been evaluated if the adsorption of chromium(VI) into the MWCNTs must be considered as a liquid-solid phase reaction which includes diffusion of chromium species from the aqueous phase to the adsorbent surface, the diffusion of ions within the nanotubes and the chemical reaction between ions and any functional group in the carbon nanotubes [19]. The rate equations for the above three cases are:

i. film-diffusion controlled process, in which the rate equation is

$$\ln(1 - F) = -kt \quad (3)$$

ii. particle-diffusion controlled process, with the equation as

$$\ln(1 - F^2) = -kt \quad (4)$$

iii. Shrinking core model

$$3 - 3(1 - F)^{2/3} - 2F = kt \quad (5)$$

In all the above equations, F is the fractional approach to equilibrium, which is defined as

$$F = \frac{[Cr]_{c,t}}{[Cr]_{c,e}} \quad (6)$$

whereas k is the corresponding rate constant.

## 2.4 Modeling of adsorption isotherms

Both the Langmuir and Freundlich approaches had been used to model the experimental data, being both widely used in the modeling of adsorption or ion exchange processes [20].

The Langmuir model is valid for monolayer adsorption onto a surface containing a limited number of identical sites. The equation in its linear form describing this model is

$$\frac{1}{[Cr]_{c,e}} = \frac{1}{[Cr]_{c,m}} + \frac{1}{b[Cr]_{c,m}} \frac{1}{[Cr]_{s,e}} \quad (7)$$

where b is a constant related to the model,  $[Cr]_{c,m}$  is the maximum metal uptake in the carbon nanotubes and  $[Cr]_{s,e}$  is the equilibrium chromium(VI) concentration in the solution.

The Freundlich model is an empirical expression describing adsorption onto heterogeneous surfaces, having the adsorbent surface sites with a variation of binding energies. In this case, the equation also in its linear form is

$$\ln[Cr]_{c,e} = \ln k_f + \frac{1}{n} \ln[Cr]_{s,e} \quad (8)$$

where  $k_f$  and n are parameters related to the Freundlich model.

## 3. Results and discussion

### 3.1 Effect of stirring speed

Adsorption of chromium(VI) from aqueous solution to MWCNTs as a function of the stirring speed at pH  $1 \pm 0.1$  is shown in **Figure 1**. The adsorption of chromium(VI) increases with increasing stirring speed, though from  $1000 \text{ min}^{-1}$  no significant

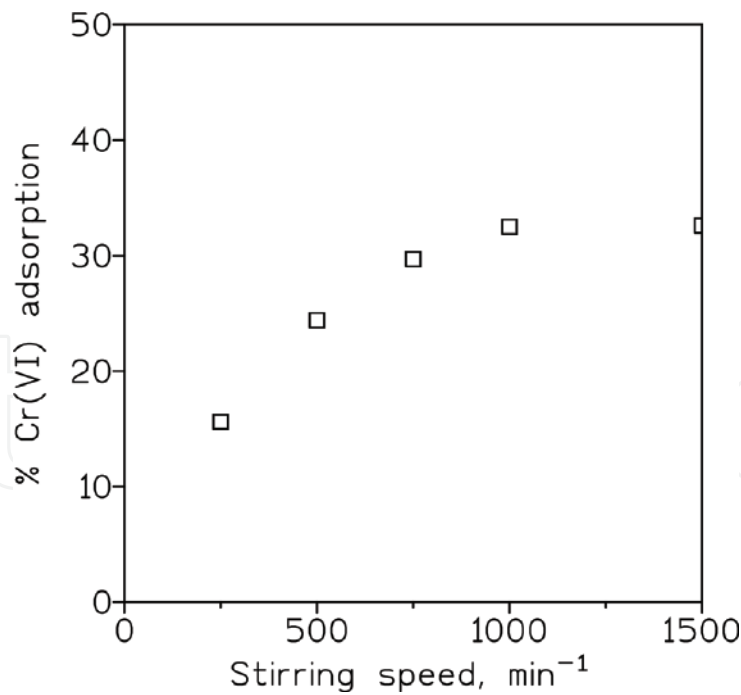


**Figure 1.** Influence of stirring speed on the percentage of chromium(VI) adsorption at the equilibrium. Aqueous solution: 0.01 g/L Cr(VI). MWCNTs dosage: 1 g/L. Temperature: 20°C. Time: 2 h.

changes are encountered in metal adsorption specially at the longer contact times. These results shown that from 1000 min<sup>-1</sup>, the thickness of the aqueous diffusion layer and the aqueous resistance to mass transfer were minimized, and the diffusion contribution of the aqueous species to the adsorption process is assumed to be constant.

### 3.2 Effect of temperature

The relationship between chromium(VI) adsorption and the temperature is also studied using aqueous solutions containing 0.01 g/L Cr(VI) at pH 4 ± 0.1 and adsorbent dosage of 1 g/L. **Table 2** shows the variation of log D<sub>Cr</sub> vs. T, over the range of temperatures used, where D (the distribution coefficient) was calculated as

$$D = \frac{[Cr]_{c,e}}{[Cr]_{s,e}} \quad (9)$$

where [Cr]<sub>c,e</sub> and [Cr]<sub>s,e</sub> being the chromium concentrations in the nanotubes and in the aqueous solution at equilibrium. There is a decrease of chromium adsorption with the increase of temperature. One explanation of these results is to consider the nature of the species with the temperature as predicted by the Bjerrum equation. Accordingly, the estimated change of enthalpy is -14 kJ/mol, and the adsorption process is therefore exothermic.

Temperature	% adsorption	D (L/g)	Log D
20°C	44	0.79	-0.10
40°C	36	0.56	-0.25
60°C	28	0.39	-0.41

Stirring speed: 1000 min<sup>-1</sup>. Time: 2 h.

**Table 2.** Influence of temperature on chromium(VI) adsorption onto the MWCNTs.

The kinetic adsorption data were simulated with the two models shown in Eqs. (1) and (2), representing the pseudo-first- and pseudo-second-order models, respectively. The results are listed in **Table 3**. From the values of  $r^2$ , the kinetic adsorption of chromium(VI) at the temperatures of 20 and 60°C can be fitted by the pseudo-second-order model.

### 3.3 Effect of pH

The pH of the aqueous solution may be one of the most decisive parameters controlling the adsorption process. The influence of pH on the adsorption of chromium(VI) is investigated at pH values ranging from 1 to 13. **Figure 2** shows that the maximum adsorption of the metal occurs at pH 4, and decreases either at more acidic and at alkaline pH values, these mean that  $\text{HCrO}_4^-$  species (which is predominant at this range of initial chromium(VI) concentration and pH values below 6) is adsorbed onto the MWCNTs better than  $\text{CrO}_4^{2-}$  species, which is predominant at alkaline pH values. Furthermore, **Table 4** presented data about the adsorption of 0.005 g/L chromium(VI) at pH values of 1 and 4; it is also observed how the percentage of metal adsorption is greatly dependent on the pH of the aqueous solution, decreasing as the pH shifts to more acidic values.

### 3.4 Effect of carbon nanotubes dosage

It is apparent that the amount of adsorbent used in the removal of a given solute from aqueous solutions is critical for the practical application of such system. Thus, adsorption of chromium(VI) as a function of MWCNT dosages at  $\text{pH } 4 \pm 0.1$  is shown in **Figure 3**. The percentage of metal adsorption increases with the MWCNT dosage increasing, i.e. near 90% chromium(VI) is adsorbed at the adsorbent dosage of 10 g/L and this value down until 44% when the adsorbent dose is 1 g/L. These results are consistent with the fact that the increase of the adsorbent dosage results in the increase of the active sites in which the metal can be adsorbed, thus increasing the percentage of metal adsorbed or eliminated from the aqueous solution.

The data of the amount of chromium(VI) adsorbed on the MWCNTs (mg/g) and the metal concentration remaining in solution (mg/L) are fitted to the Langmuir and Freundlich models represented by Eqs. (7) and (8), respectively. The relative parameters obtained from the fit are listed in **Table 5**. The experimental data are well described by both models, indicating that the chromium(VI) uptake onto the MWCNTs is homogeneous and multilayer in nature. However, a singular fact of the Langmuir model can be described by the dimensionless separation factor, defined as

$$R = \frac{1}{1 + b[\text{Cr}]_{s,0}} \quad (10)$$

		20°C	60°C
Pseudo-first order	$k_1$ ( $\text{min}^{-1}$ )	0.057	0.056
	$r^2$	0.9493	0.9856
Pseudo-second order	$k_2$ (g/min mg)	0.16	0.034
	$r^2$	0.9992	0.9983

**Table 3.** Constants for the kinetic adsorption of chromium(VI) to MWCNTs using different adsorption models.

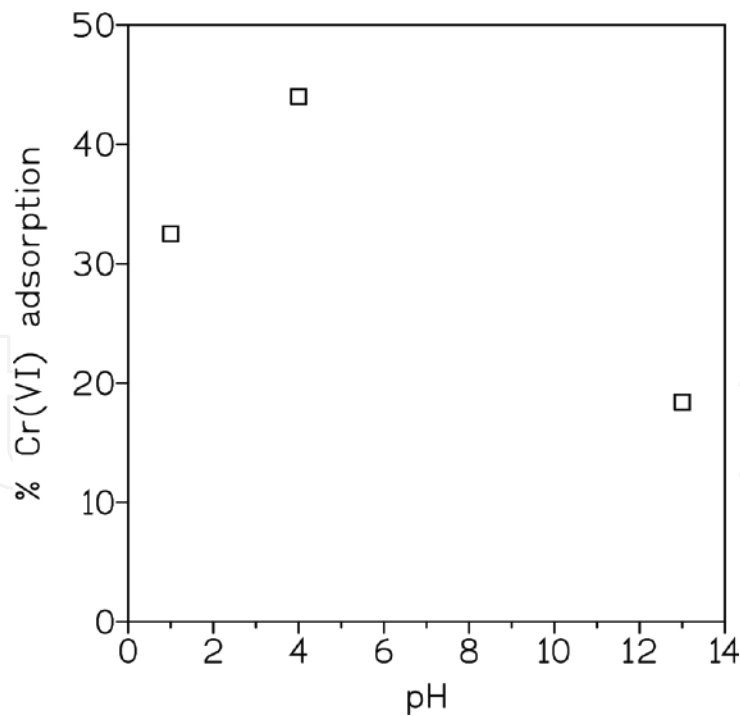


**Figure 2.**  
 Influence of the pH on chromium(VI) adsorption. Experimental conditions as in Figure 1.

pH $\pm$ 0.1	% adsorption
1	19.5
2	80.7
3	91.1
4	99.5

MWCNTs dosage: 10 g/L. Temperature: 20°C. Time: 2 h.

**Table 4.**  
 Influence of pH on chromium(VI) adsorption onto the MWCNTs.

where  $[Cr]_{s,0}$  is the initial metal concentration in the solution and  $b$  is the Langmuir constant. The value of  $R$  indicates if the adsorption is unfavorable ( $R > 1$ ), linear ( $R = 1$ ), favorable ( $0 < R < 1$ ) or irreversible ( $R = 0$ ). The value of  $R$  in this investigation was found to be 0.82, indicating that the adsorption of chromium(VI) is favorable.

### 3.5 Effect of metal concentration

The various adsorptions of chromium(VI) on MWCNTs as a function of initial metal concentration at pH  $4 \pm 0.1$  are shown in Figure 4. The adsorption percentage of chromium(VI) decreases with initial metal concentration increasing.

The rate law governing the metal adsorption was investigated using the three models depicted in Eqs. (3)–(5), and the results from these fits were summarized in Table 6. It can be seen that within the particle-diffusion controlled model, the chromium(VI) adsorption onto the MWCNTs was better explained.

### 3.6 Comparison with other adsorbent-anion exchangers

The adsorption capacity, in terms of percentage of adsorption, found in this investigation was compared with the results obtained using other potential adsorbent-anion exchangers for Cr(VI). The results obtained from this set of

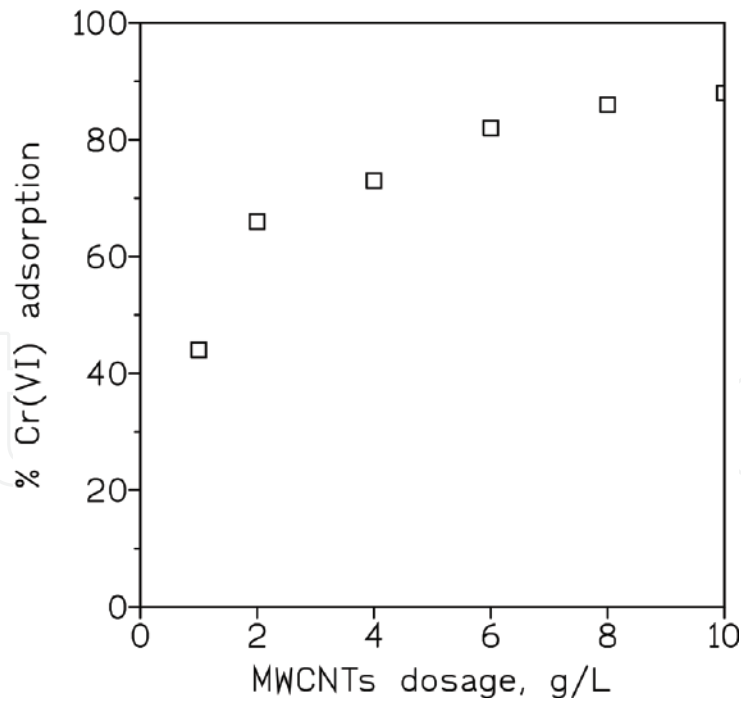


**Figure 3.**  
Influence of MWCNTs dosage on chromium(VI) adsorption. Aqueous solution: 0.01 g/L Cr(VI) at pH 4. Temperature: 20°C. Time: 2 h.

	b (L/mg)	[Cr] <sub>e,m</sub> (mg/g)	r <sup>2</sup>	ln k <sub>f</sub>	1/n	r <sup>2</sup>
Langmuir	0.021	37	0.9950			
Freundlich				-0.28	0.94	0.9952

**Table 5.**  
Langmuir and Freundlich constants.

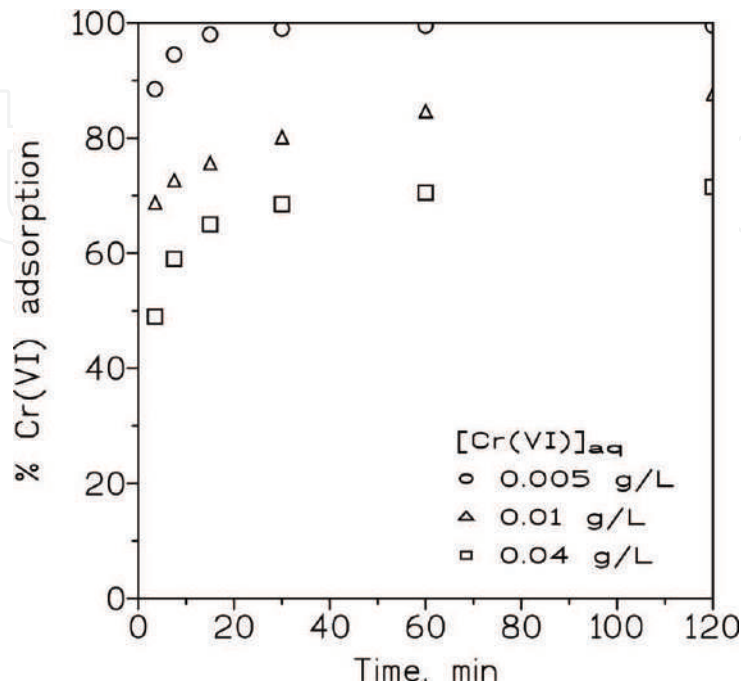


**Figure 4.**  
Influence of initial chromium(VI) concentration on metal adsorption. MWCNTs dosage: 10 g/L. Temperature: 20°C.

Equation		0.005 g/L	0.01 g/L	0.04 g/L
3	k (min <sup>-1</sup> )	0.48	0.27	0.26
	r <sup>2</sup>	0.9008	0.7710	0.8968
4	k (min <sup>-1</sup> )	0.36	0.14	0.15
	r <sup>2</sup>	0.9537	0.9739	0.9796
5	k (min <sup>-1</sup> )	0.11	0.06	0.06
	r <sup>2</sup>	0.9004	0.8767	0.9760

**Table 6.**  
 The rate law governing the adsorption of chromium(VI) onto the MWCNTs.

experiments together with the experimental conditions used in the investigation were summarized in **Table 7**.

It can be concluded that, under the present experimental conditions, Dowex 1×8 resin is the most effective to remove hazardous chromium(VI) from near neutral or acidic solutions, whereas MWCNTs presented the worse registers. The above is not a bad conclusion about the use of these MWCNTs as adsorbents for Cr(VI), and not delegitimize the investigation presented in this work, only stated that there are other potential adsorbents-ion exchangers that remove Cr(VI) from liquid effluents with a better efficiency.

### 3.7 Thermodynamics

Besides the data of the change of enthalpy (see Section 3.5) derived for the adsorption process of chromium(VI) onto the carbon nanotubes, a further thermodynamic analysis of the adsorption process can be considered taking into account the next equations:

$$\Delta G^\circ = -RT \ln b \quad (11)$$

$$\Delta G^\circ = \Delta H^\circ - T\Delta S^\circ \quad (12)$$

Accordingly with Eq. (11) in which b is the Langmuir constant showed in **Table 5**, it can be obtained that the value of  $\Delta G^\circ$  is 9 kJ/mol, confirming that the chromium(VI) uptake onto the nanotubes is nonspontaneous.

To calculate  $\Delta S^\circ$  for the present adsorption system, Eq. (12) is used, obtaining a value of  $-0.08$  kJ/mol K. The negative value for the change of entropy characterizes a decrease disorder of the system when chromium(VI) is adsorbed onto the nanotubes.

Adsorbent-anion exchanger	Active group	pH 1	pH 4
Dowex 1x8	QAS-Cl <sup>-</sup> form	89	>99
MWCNTs	None	32	42
ox-MWCNTs	-COOH	68	No data
Activated carbon	None	47	59

Aqueous solution: 0.01 g/L Cr(VI) at different pH values. Solid dosage: 1 g/L. Temperature: 20°C. Stirring speed: 1000 min<sup>-1</sup>. Time: 1 h.  
 QAS: quaternary ammonium salt.

**Table 7.**  
 Percentage of Cr(VI) adsorption using various adsorbent-anion exchangers.

### 3.8 Chromium(VI) desorption

In the present investigation, the desorption of chromium(VI) from the metal-loaded carbon nanotubes was studied using hydrazine sulfate solutions as desorbent for the metal, at the same time, in the desorption process, Cr(VI) is reduced to the less hazardous Cr(III) oxidation state, accordingly to



Desorption experiments were carried out with aqueous solutions containing 25–50 g/L of hydrazine sulfate and 2 mg/g Cr(VI)-loaded MWCNTs at a 25 mL/g solution volume/weighed MWCNTs relationship and 20°C. The results from these experiments indicated that:

- i. The variation in the hydrazine sulfate solution concentration has no effect on the reaction yield (95% chromium recovery from loaded nanotubes).
- ii. The equilibrium is reached within 5 min of reaction.
- iii. The desorbed solution contained a chromium(III) concentration near eight times the initial chromium(VI) concentration in the feed solution (0.01 g/L) of the adsorption experiments.

## 4. Conclusions

The adsorption of chromium(VI) onto the multi-walled carbon nanotubes is dependent on the pH values of the aqueous solution. The adsorption reaches a maximum at pH 4 and decreases at more acidic and alkaline pH values. The adsorption is exothermic ( $\Delta H^\circ = -14$  kJ/mol) and nonspontaneous (positive  $\Delta G^\circ$  valor), whereas at 20–60°C, the adsorption of chromium (VI) onto the nanotubes better fits to the pseudo-second-order model. In the 0.005–0.04 g/L range of chromium(VI) concentrations in the aqueous solution, the metal uptake onto the nanotubes responded well to the particle-diffusion model, and the metal adsorption responded to the Langmuir and Freundlich isotherms, indicating that the adsorption process is homogeneous and multilayer in nature. Chromium(VI) can be desorbed from MWCNTs by the use of hydrazine sulfate solutions, which releases to the aqueous solution chromium in the less hazardous (III) valence state.

## Acknowledgements

This research was funded by the Ministry of Science, Innovation and Universities of the Spanish Government, in the “Challenges collaboration” call for proposals in 2017 (Ref. RTC-2017-6629-5).

## Conflict of interest

The authors declare no conflicts of interest.

IntechOpen

IntechOpen

### **Author details**

Francisco J. Alguacil and Félix A. Lopez\*  
National Center for Metallurgical Research (CENIM), Spanish National Council for Scientific Research (CSIC), Madrid, Spain

\*Address all correspondence to: [f.lopez@csic.es](mailto:f.lopez@csic.es)

### **IntechOpen**

---

© 2019 The Author(s). Licensee IntechOpen. This chapter is distributed under the terms of the Creative Commons Attribution License (<http://creativecommons.org/licenses/by/3.0>), which permits unrestricted use, distribution, and reproduction in any medium, provided the original work is properly cited. 

## References

- [1] Alguacil FJ, Alonso M, Lopez FA, Lopez-Delgado A. Pseudo-emulsion membrane strip dispersion (PEMSD) pertraction of chromium (VI) using Cyphos IL101 ionic liquid as carrier. *Environmental Science and Technology*. 2010;**44**:7504-7508. DOI: 10.1021/es101302b
- [2] Wang Y, Li Y, Zhong Y, Cui C. Chromium(VI) removal by tri-n-octylamine/n-heptane via a pseudo-emulsion-based hollow fiber strip dispersion technique. *Desalination and Water Treatment*. 2017;**63**:103-112. DOI: 10.5004/dwt.2017.20150
- [3] Koubaissy B, Toufaily J, Cheikh S, Sayed Hassan M, Hamieh T. Valorization of agricultural waste into activated carbons and its adsorption characteristics for heavy metals. *Central European Journal of Engineering*. 2014;**4**:90-99. DOI: 10.2478/s13531-013-0148-z
- [4] Li Y, Cui C. Extraction behavior of Cr(VI) and coexistence with interfering ions by trialkylamine. *Journal of Water Reuse and Desalination*. 2015;**5**:494-504. DOI: 10.2166/wrd.2015.110
- [5] Bayramoglu G, Akbulut A, Yakup Arica M. Aminopyridine modified *Spirulina platensis* biomass for chromium(VI) adsorption in aqueous solution. *Water Science and Technology*. 2016;**74**:914-926. DOI: 10.2166/wst.2016.281
- [6] Garza-González MT, Ramírez-Vázquez JE, García-Hernández MA, Cantú-Cárdenas ME, Liñan-Montes A. Reduction of chromium (VI) from aqueous solution by biomass of *Cladosporium cladosporioides*. *Water Science and Technology*. 2018;**76**:2494-2502. DOI: 10.2166/wst.2017.427
- [7] Al Dwairi R. Modeling of chromium (VI) adsorption from aqueous solutions using Jordanian zeolitic tuff. *Water Science and Technology*. 2017;**75**:2064-2071. DOI: 10.2166/wst.2017.065
- [8] Elyahyaoui A, Ellouzi K, Al Zabadi H, Razzouki B, Bouhlassa S, Azzaoui K, et al. Adsorption of chromium(VI) on calcium phosphate: Mechanisms and stability constants of surface complexes. *Applied Sciences*. 2017;**7**:222. DOI: 10.3390/app.7030222
- [9] Wojcik G, Hubicki Z. Investigations of chromium(VI) ion sorption and reduction on strongly basic anion exchanger. *Separation Science and Technology*. 2018;**53**:1088-1096. DOI: 10.1080/01496395.2017.1335323
- [10] Xing J, Shen Y, Yang B, Feng D, Wang W. A green method based on electro-assisted and photo-assisted regeneration for removal of chromium(VI) from aqueous solution. *Water Science and Technology*. 2018;**76**:896-902. DOI: 10.2166/wst.2018.260
- [11] Naghizadeh A. Comparison between activated carbon and multiwall carbon nanotubes in the removal of cadmium(II) and chromium(VI) from water solutions. *Journal of Water Supply: Research and Technology-AQUA*. 2015;**64**:64-73. DOI: 10.2166/aqua.2014.022
- [12] Alguacil FJ, Garcia-Diaz I, Lopez FA, Rodriguez O. Removal of Cr(VI) and Au(III) from aqueous streams by the use of carbon nano-adsorption technology. *Desalination and Water Treatment*. 2017;**63**:351-356. DOI: 10.5004/dwt.2017.0264
- [13] Anastopoulos I, Anagnostopoulos VA, Bhatnagar A, Mitropoulos ACM, Kyzas GZ. A review of chromium removal by carbon nanotubes. *Chemistry and Ecology*. 2017;**33**:572-588. DOI: 10.1080/02757540.2017.1328503

[14] Xing J, Zhu C, Chowdhury I, Tian Y, Du D, Lin Y. Electrically switched ion exchange based on polypyrrole and carbon nanotube nanocomposite for the removal of chromium(VI) from aqueous solution. *Industrial and Engineering Chemistry Research*. 2018b;**57**:768-774. DOI: 10.1021/acs.iecr.7b03520

[15] Alguacil FJ, Lopez FA, Rodriguez O, Martinez-Ramirez S, Garcia-Diaz I. Sorption of indium (III) onto carbon nanotubes. *Ecotoxicology and Environmental Safety*. 2016;**130**:81-86. DOI: 10.1016/j.ecoenv.2016.04.008

[16] Alguacil FJ, Escudero E. The removal of toxic metals by ion exchange resins. Part VIII: Arsenic(III)/OH<sup>-</sup>/Dowex 1x8. *Revista de Metalurgia*. 2018;**54**:e132. DOI: 10.3989/revmetalm.132

[17] Alguacil FJ, Alcaraz L, Garcia-Diaz I, Lopez FA. Removal of Pb<sup>2+</sup> in wastewater via adsorption onto an activated carbon produced from winemaking waste. *Metals*. 2018;**8**:697. DOI: 10.3390/met8090697

[18] Largitte L, Pasquier R. A review of the kinetics adsorption models and their application to the adsorption of lead on an activated carbon. *Chemical Engineering Research and Design*. 2016;**109**:495-504. DOI: 10.1016/j.cherd.2016.02.006

[19] Diaz-Pavon AL, Cerpa A, Alguacil FJ. Processing of indium(III) solutions via ion exchange with Lewatit K-2621 resin. *Revista de Metalurgia*. 2014;**50**:e010. DOI: 10.3989/revmetalm.010

[20] Alguacil FJ. The removal of toxic metals by ion exchange resins. Part III: Cu<sup>2+</sup>/sulphate/Amberlite 200. *Revista de Metalurgia*. 2003;**39**:205-209. DOI: 10.3989/revmetalm.2003.v39.i3.330